REPORT DOCUMENTATION PAGE

Form Approved
OMB No. 0704-0188

Public reporting burden for this collection of information is estimated to average 1 hour per response, including the time for reviewing instructions, searching existing data sources, gathering and maintaining the data needed, and completing and reviewing this collection of information. Send comments regarding this burden estimate or any other aspect of this collection of information, including suggestions for reducing this burden to Department of Defense, Washington Headquarters Services, Directorate for Information Operations and Reports (0704-0188), 1215 Jefferson Davis Highway, Suite 1204, Arlington, VA 22202-4302. Respondents should be aware that notwithstanding any other provision of law, no person shall be subject to any penalty for failing to comply with a collection of information if it does not display a currently valid OMB control number. **PLEASE DO NOT RETURN YOUR FORM TO THE ABOVE ADDRESS.**

1. REPORT DATE *(DD-MM-YYYY)*	2. REPORT TYPE	3. DATES COVERED *(From - To)*
January 2014	Journal Article	January 2014-April 2014

4. TITLE AND SUBTITLE

Evaluating Ionic Liquids as Hypergolic Fuels: Exploring Reactivity from Molecular Structure†

5a. CONTRACT NUMBER
FA9300-11-C-3004

5b. GRANT NUMBER

5c. PROGRAM ELEMENT NUMBER

6. AUTHOR(S)

Parker D. McCrary, Gregory Chatel, Spencer A. Alaniz, O. Andreea Cojocaru, Preston A. Beasley, Luis A. Flores, Steven P. Kelley, Patrick S. Barber, and Robin D. Rogers

5d. PROJECT NUMBER

5e. TASK NUMBER

5f. WORK UNIT NUMBER
Q0QH

7. PERFORMING ORGANIZATION NAME(S) AND ADDRESS(ES)

Air Force Research Laboratory (AFMC)
AFRL/RQRP
10 E. Saturn Blvd.
Edwards AFB, CA, 93524-7680

8. PERFORMING ORGANIZATION REPORT NO.

9. SPONSORING / MONITORING AGENCY NAME(S) AND ADDRESS(ES)

Air Force Research Laboratory (AFMC)

AFRL/RQR
5 Pollux Drive.
Edwards AFB, CA, 93524-7048

10. SPONSOR/MONITOR'S ACRONYM(S)

11. SPONSOR/MONITOR'S REPORT NUMBER(S)

AFRL-RQ-ED-JA-2014-044

12. DISTRIBUTION / AVAILABILITY STATEMENT
Approved for public release; distribution unlimited

13. SUPPLEMENTARY NOTES
Journal article published in the ACS Energy & Fuels, Vol. #28, Issue #5, March 2014.
PA Case Number: #14116; Clearance Date: 17 Mar 14.
© 2014 American Chemical Society
The U.S. Government is joint author of the work and has the right to use, modify, reproduce, release, perform, display, or disclose the work.

14. ABSTRACT
Thirty eight ionic liquids (19 of which are new) comprised of thirteen cations, 1-propargyl-3-methyl-imidazolium, 1-allyl-3-methyl-imidazolium, 1,3-dimethyl-imidazolium, 1-ethyl-3-methyl-imidazolium, 1-butyl-3-methyl-imidazolium, 1-methoxyethyl-3-methyl-imidazolium, 1-methyl-4-butyl-1,2,4-triazolium, 1-methyl-4-allyl-1,2,4-triazolium, 1-methyl-4-amino-1,2,4-triazolium, *N*-butyl-*N*-methyl-pyrrolidinium, *N*-allyl-*N*-methyl-pyrrolidinium, *N*-allyl-pyridinium, and *N*-butyl-3-methyl-pyridinium paired with three anions, dicyanamide, azide, and nitrocyanamide, have been prepared, characterized, and evaluated as potential hypergolic fuels by determining key physical, thermal, and ignition properties. The reactivity of these ionic liquids (32 liquids and 6 solids which melt below 100 °C) was strongly correlated to increased electron density in the cation, while small changes in physical properties had little effect beyond a certain threshold, suggesting that subtle changes in chemical reactivity can greatly influence the hypergolic ignition pathway.

15. SUBJECT TERMS

16. SECURITY CLASSIFICATION OF:

a. REPORT	b. ABSTRACT	c. THIS PAGE
Unclassified	Unclassified	Unclassified

17. LIMITATION OF ABSTRACT
SAR

18. NUMBER OF PAGES
43

19a. NAME OF RESPONSIBLE PERSON
G. Vaghjiani

19b. TELEPHONE NO
(include area code)
661-275-5657

Standard Form
298 (Rev. 8-98)
Prescribed by ANSI
Std. 239.18

Evaluating Ionic Liquids as Hypergolic Fuels: Exploring Reactivity from Molecular Structure†

Parker D. McCrary, Gregory Chatel,‡ Spencer A. Alaniz, O. Andreea Cojocaru, Preston A. Beasley,§ Luis A. Flores, Steven P. Kelley, Patrick S. Barber, and Robin D. Rogers*

Center for Green Manufacturing and Department of Chemistry, The University of Alabama, Box 870336, Tuscaloosa, AL 35487, USA

‡Current Address: Institut de Chimie des Milieux et Matériaux de Poitiers (IC2MP), CNRS/Université de Poitiers, ENSIP, Bat. B1, 1 rue Marcel Doré, 86073 Poitiers Cedex 9, France.

§Current Address: Power Systems and Environmental Research, Southern Research Institute, 2000 Ninth Ave. S., Birmingham, AL 35205, USA

*Corresponding Author: RDRogers@ua.edu

Abstract

Thirty eight ionic liquids (19 of which are new) comprised of thirteen cations, 1-propargyl-3-methyl-imidazolium, 1-allyl-3-methyl-imidazolium, 1,3-dimethyl-imidazolium, 1-ethyl-3-methyl-imidazolium, 1-butyl-3-methyl-imidazolium, 1-methoxyethyl-3-methyl-imidazolium, 1-methyl-4-butyl-1,2,4-triazolium, 1-methyl-4-allyl-1,2,4-triazolium, 1-methyl-4-amino-1,2,4-triazolium, *N*-butyl-*N*-methyl-pyrrolidinium, *N*-allyl-*N*-methyl-pyrrolidinium, *N*-allyl-pyridinium, and *N*-butyl-3-methyl-pyridinium paired with three anions, dicyanamide, azide, and nitrocyanamide, have been prepared, characterized, and evaluated as potential hypergolic fuels by determining key physical, thermal, and ignition properties. The reactivity of these ionic liquids (32 liquids and 6 solids which melt below 100 °C) was strongly correlated to increased electron density in the cation, while small changes in physical properties had little effect beyond a certain threshold, suggesting that subtle changes in chemical reactivity can greatly influence the hypergolic ignition pathway.

Introduction

Ionic liquids (ILs, generally defined as salts with melting points below 100 $^{\circ}$C[1]) have been previously proposed as hypergolic fuels[2] for the replacement of hydrazine based on inherent and designable properties, such as low volatility and favorable transport properties. While many IL-forming anions (*e.g.*, dicyanamide ([N(CN)$_2$]$^-$ abbreviated here as [DCA]$^-$),[3] nitrocyanamide ([N(CN)(NO$_2$)]$^-$ abbreviated here as [NCA]$^-$),[4] and dicyanoborohydride ([B(CN)$_2$H$_2$]$^-$)[5]) have been shown to be hypergolic (*i.e.*, exhibit spontaneous ignition upon contact with an oxidizer[6]) with nitric acid[3-5] or hydrogen peroxide,[7] many other practical properties must also be considered in the design of hydrazine replacements.

Currently, the basic design strategy to make hypergolic ILs is to incorporate reactivity in the cation and/or anion through the incorporation of chemical bonds known to induce a hypergolic reaction with common oxidizers, such as the N-C≡N bond (*e.g.*, in [DCA]$^-$) or B-H bonds (*e.g.*, in the [B(CN)$_2$H$_2$]$^-$ anion[5] or the boronium[8] cation). Even with this designed reactivity, many other physical and chemical properties, such as viscosity[9] or density,[10] play a large role in the mixing, ignition, and combustion processes that occur upon contact. However, much of the focus in the literature to date has been on the synthetic development of new hypergolic ILs to improve upon deficiencies in previous systems.[2-5,7,8] As a result, it is hard to predict which cations should be paired with already known hypergolic anions and whether the modified physical properties or the introduced functional groups are responsible for any enhanced reactivity.

Here we present experimental data which might be used to provide reliable models which would allow a design strategy for the improvement of ignition delays in hypergolic ILs. We have explored whether incorporation of enhanced reactivity into an IL cation paired with the known hypergolic anions [DCA]$^-$, [NCA]$^-$, and azide ([N$_3$]$^-$) (**Figure 1**) would result in improved hypergolic reactivity as a result of new chemical functionality in the cation or as a result of changed physical properties (*e.g.*, viscosity). Of these, the [DCA]$^-$ anion is the most well studied[11-15] with a published ignition pathway[11,13] and kinetic combustion studies.[15] ILs containing the [N$_3$]$^-$ and [NCA]$^-$ anions[4,16,17] have also been previously shown to exhibit reactivity or hypergolicity with white fuming nitric acid (WFNA). The IL cations were chosen based on heterocycle precursors known to form low melting salts (*e.g.*, imidazole, 1,2,4-triazole, pyrrolidine, and pyridine) functionalized with alkyl, alkenyl, alkynyl, or N-N groups (**Figure 1**).
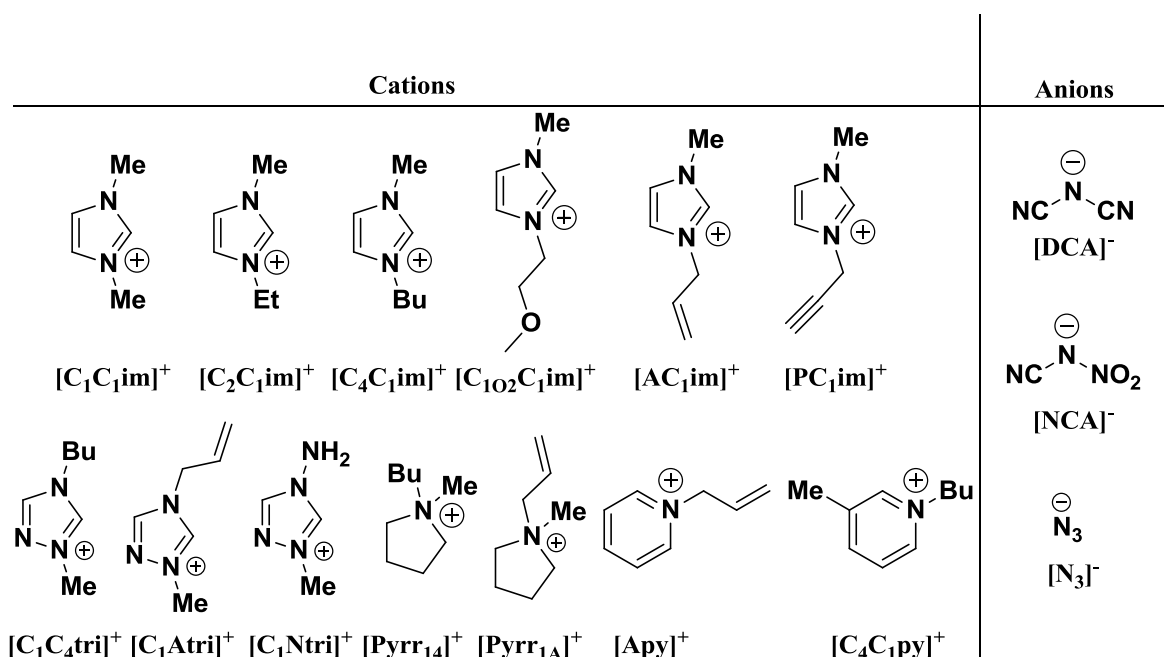
Figure 1. Energetic and/or hypergolic cation and anion combinations selected for this study.

Results and Discussion

Syntheses. Thirteen halide salt precursors were synthesized through typical quaternization reactions[5,18-27] between the neutral heterocycles and respective alkylating agents, such as iodomethane, chloroethane, 1-chlorobutane, 1-bromobutane, 1-chloro-2-methoxyethane, allyl chloride, and propargyl bromide (**Scheme 1**). A typical quaternization reaction was conducted by first dropwise adding 1.1 molar excess of the alkylating agent under a constant stream of argon to a round bottom flask containing the pure heterorcycle while being stirred at 0 °C. The reaction was then slowly heated to a gentle reflux for between 24 and 96 h and monitored by ^{1}H NMR until no unreacted heterocycle was detected. In the case of the reaction between propargyl bromide and 1-methyl-imidazole, a small amount of acetonitrile was added to the flask containing the heterocycle to help dissipate some of the heat generated upon addition. For the reactions between iodomethane, allyl chloride, or butyl chloride with 1-methyl-1,2,4-triazole, 4-amino-1,2,4-triazole, 1-methyl-pyrrolidine, pyridine, and 3-methyl-pyridine, acetonitrile was added as a solvent because either the starting heterocycle is a solid at 0 °C (1-methyl-1,2,4-triazole, 4-amino-1,2,4-triazole, or 1-methyl-pyrrolidine) or the subsequent halide salt was previously reported to have too high of a melting point to remain a liquid at the reflux temperature (*e.g.*, the pyridindium-based halide salts).[25-27] In each case where acetonitrile was

added as a solvent, the halide could be easily precipitated from solution upon the addition of ethyl acetate to the solution.
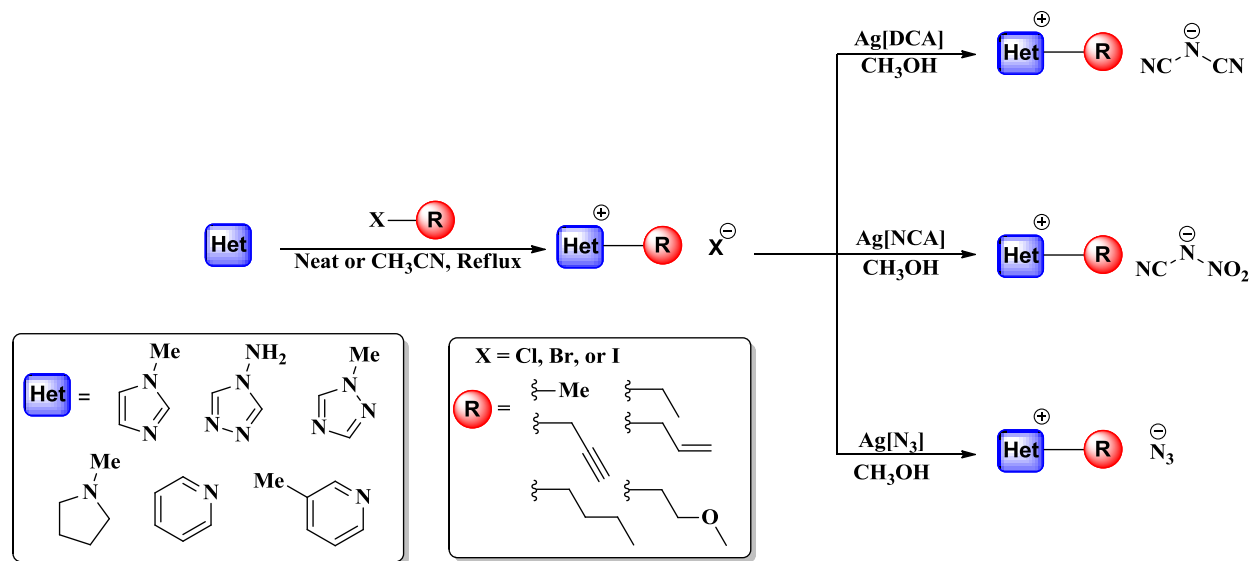
Scheme 1. Overall synthetic pathway for the synthesis of the ILs *via* silver salt metathesis.

The anion precursors Ag[DCA] and Ag[N$_3$] were prepared through a stoichiometric reaction between saturated aqueous solutions of either Na[DCA] or Na[N$_3$] with Ag[NO$_3$] which immediately resulted in the precipitation of the respective silver salts from water. Na[NCA] was generated *in situ* from the reaction of *N*-methyl-*N*-nitroso-*N'*-nitro-guanidine with NaOH. The resulting basic solution was neutralized with HNO$_3$ and a saturated solution of AgNO$_3$ was then added to yield the precipitation of Ag[NCA].[4] Due to the potential shock sensitivity of the synthesized silver salts, special care was taken to not isolate more than 25 mmol at any given time and to constantly keep the salts stored as a suspension in methanol.

Saturated solution of the halide precursors in methanol were added to the suspensions of a 1.1 molar excess of the corresponding silver salt described above. The mixtures were then allowed to stir at 25 ^{o}C for at least 3 days while completely covered by aluminum foil to prevent light oxidation.[3] The metathesis reactions were monitored *via* ^{1}H NMR by observing the upfield shift of the azolium peaks until only a single set of cation peaks were present. The presence of the anion was confirmed *via* ^{13}C NMR and Fourier Transform Infrared Spectroscopy (FTIR; see ESI). The resulting silver halide salts were removed by double filtration through a Teflon filter and methanol was removed by reduced pressure at 40 ^{o}C to yield the desired products as

nonviscous liquids or solids.   Additionally, a $AgNO_3$ test was performed to ensure the completeness of the metathesis reaction by adding a saturated aqueous solution of each salt to an acidified saturated solution of $AgNO_3$ to visually observe if any silver halide precipitated from the solution.

Thirty-eight salts (32 liquids and 6 solids) were isolated from thirteen cations and three anions.   The only failed metathesis reaction was the reaction between $[PC_1im]Br$ and $Ag[N_3]$, which resulted in a black tar, which could not be identified spectroscopically.   This result matched a previous report[17] where the tar was believed by the authors to be a decomposition product of a "click" reaction between the alkyne functional group in the $[PC_1im]^+$ cation and $[N_3]^-$, but this was not further investigated.

Upon the removal of excess silver salts, each isolated IL was extensively dried under high vacuum ($\sim 1 \times 10^{-4}$ torr) while being stirred and heated at 50-70 $^{\circ}C$ for between 7 and 10 d. Additionally, each salt was freeze-thawed three times to remove any entrapped gasses and trace amounts of volatiles.   The purity of each salt was evaluated by monitoring the cation-specific peaks in the ^1H and ^{13}C NMR.   Due to the lack of hydrogen atoms in each anion, ^{13}C NMR ([DCA] = 119 ppm, [NCA] = 117 ppm, and $[N_3]^-$ = no peak) and IR (see ESI†) were utilized to characterize the anion in each case.   As each IL was hygroscopic, after the extensive drying stage samples were immediately analyzed with the remainder of the compound stored under argon and sealed using a septum.   Samples were not exposed to atmospheric conditions again until the hypergolic ignition tests were conducted.

Single Crystal Analyses.   Single crystals were isolated for the precursor salt $[C_1Ntri]I$ and for four of the six solid ILs, $[C_1Ntri][N_3]$, $[C_1C_1im][N_3]$, $[C_1C_1im][NCA]$, and $[PC_1im][NCA]$. Single crystal X-ray diffraction experiments were conducted for both identification of the isolated salts and to determine if any specific trends in intermolecular contacts might provide insight into the observed melting behavior and physical properties.   Diagrams of the asymmetric units, short contacts around each ion, and packing environments are shown in **Figure 2**.

[C₁Ntri]I

[C₁Ntri][N₃]

[C$_1$C$_1$im][N$_3$]

[C$_1$C$_1$im][NCA]

[PC$_1$im][NCA]
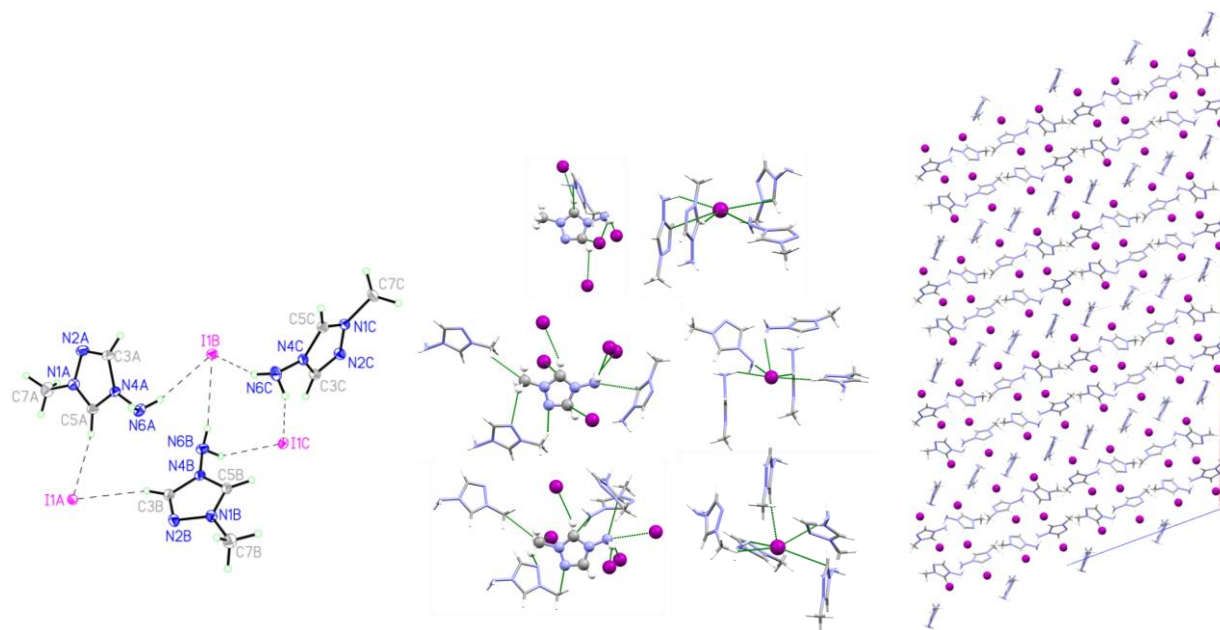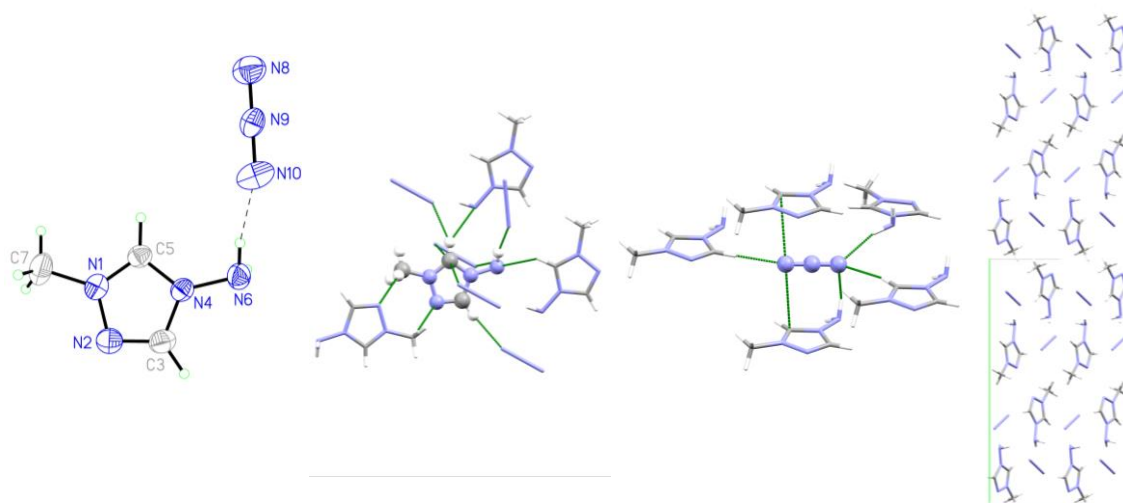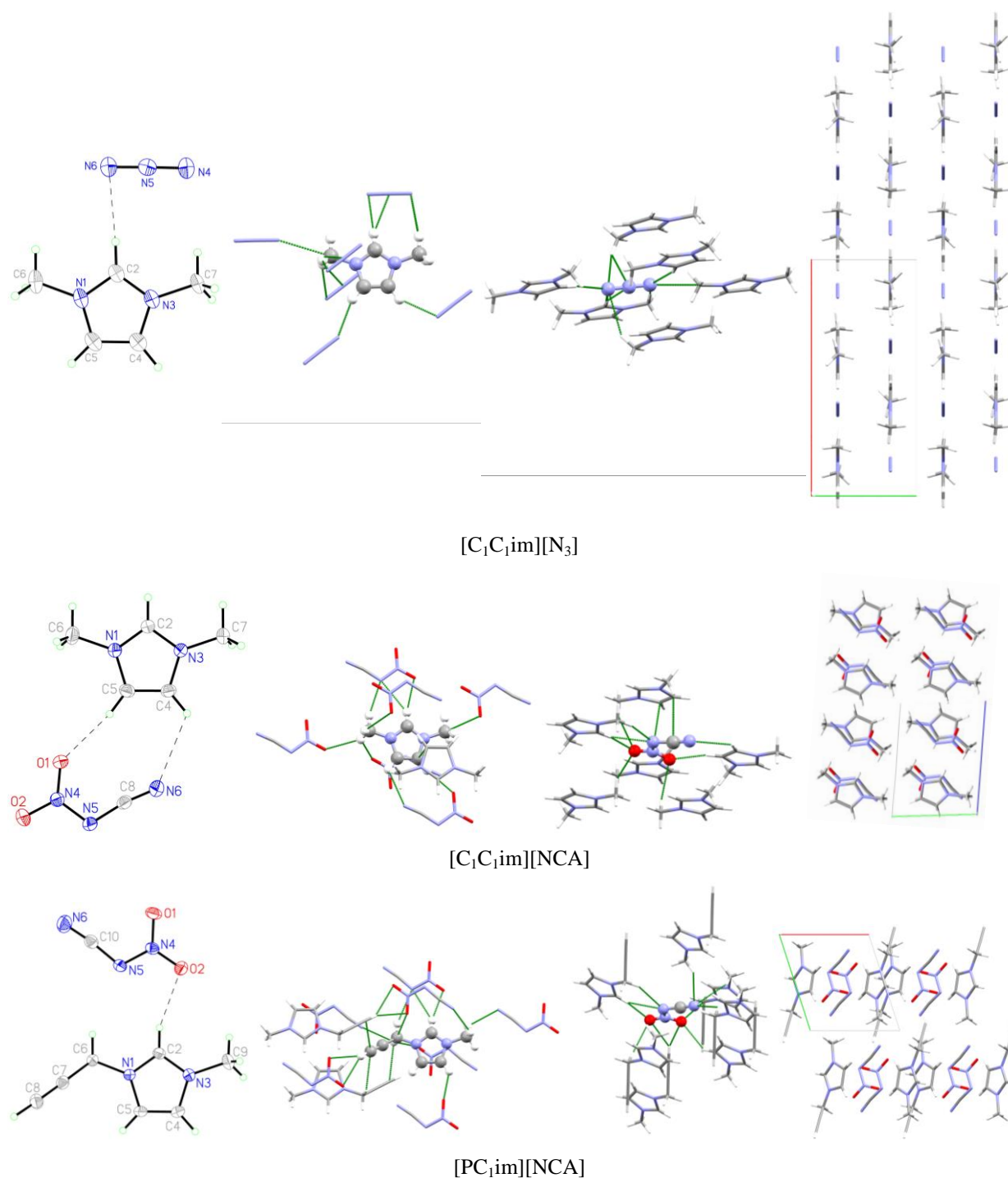
Figure 2. From left to right for each salt: 50% probability ellipsoid ORTEP diagram of the formula unit with the shortest cation-anion contact noted; short contacts (< sum of the van der Waals radii) around the cation; short contacts around the anion; and packing diagram. The disorder in [C$_1$C$_1$im][N$_3$] was omitted for clarity.

[C₁Ntri]I crystallized in the monoclinic space group *C2/c* with three symmetry-independent formula units per asymmetric unit. The three unique [C₁Ntri]⁺ ions have similar bond distances and angles, but differ by the orientation of the 4-amino group. Based on the positions of hydrogen atoms located from the difference map, the amino groups on rings A and C are oriented such that the amino lone pair eclipses C3, while on ring B the amino lone pair eclipses C5. As a result of this the three formula units cannot be reduced by crystallographic symmetry.

All three cations and anions in [C₁Ntri]I have different short contact environments with the main interactions being hydrogen bonding to the anion (especially from the amino hydrogen atoms), electrostatic stacking of the anion with the ring, and cation-cation interactions between amino lone pairs and triazolium rings. The packing appears to be mainly dominated by charge ordering of anions and cations.

The high Z' and different orientations of the amino groups, appear to be structural features which optimize N-H···I hydrogen bonding. The three unique cations interact with each other through the amino-ring interactions to form a cluster such that the amino groups lie on the vertices of a triangle with their hydrogen atoms pointing away from the center of the triangle (Figure 3). Cations B and C interact with cations on the neighboring clusters along the *c* axis, forming an infinite helix, and these helices are arranged side-by-side down the *b* axis, forming layers. Anion B is in the optimum spot for hydrogen bonding with these cation structures and accepts two strong N-H hydrogen bonds and a ring C-H hydrogen bond from one cluster and another N-H hydrogen bond from a cation cluster in the neighboring helix along *b*. Anion A packs into the cation helices alternating with Anion B and accepts one N-H bond, although it is less directional. Anion C accepts two N-H hydrogen bonds and bridges adjacent cation layers along the *a* axis, completing the 3-dimensional packing network. This arrangement allows for a large degree of cation-cation π stacking and cation-anion stacking. The triazolium rings jut out of the cation cluster like propeller blades which are able to interlace with the anions and each other (Figure 3).
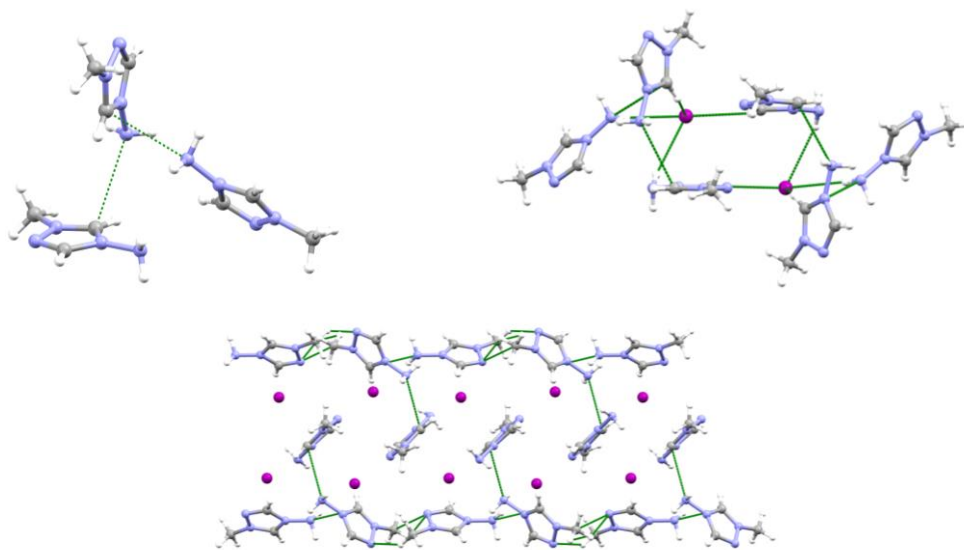
Figure 3: Packing diagrams of [C$_1$Ntri]I showing cation cluster (*top left*), anion-mediated bridges between adjacent clusters (*top right*), and side-by-side arrangement of two infinite helices of cation-cation linked clusters (*bottom*).

[C$_1$Ntri][N$_3$] crystallized in the monoclinic space group P2$_1$/*n* with one formula unit per asymmetric unit. Cation-cation hydrogen bonds are observed between ring or methyl hydrogen atoms on the donor cation and nitrogen atoms on the acceptor. The amine lone pair to azolium ring interactions found in [C$_1$Ntri]I are not present in this structure. The hydrogen atoms attached to C3, C5, and the amine functional group form hydrogen bonds with terminal nitrogen atoms on three unique azide anion molecules. Two anions interact with the C2 position through out-of-plane short contacts on either side of the ring. The packing appears to be mainly dominated by charge ordering of anions and cations. The anion molecules pack above and below the edge of the cation (N4-C5) contain the amine functional group which allows for many short contacts between terminal nitrogen atoms in the azide anion and hydrogen atoms on C3, C5, and N6.

[C$_1$C$_1$im][N$_3$] crystallized in the orthorhombic space group *Pnma*. Every non-hydrogen atom has unique coordinates, but resides on a crystallographic mirror plane so there is one half of a formula unit per asymmetric unit. Four of the cation-anion interactions are hydrogen bonds in the plane of the ring, while two are out-plane-hydrogen bonds between anions and methyl hydrogen atoms. Surprisingly, the anion stacks over the methyl group rather than the more typical position over the core of the ring. The shortest contact observed is between the most acidic proton, C2H, and N6, a terminal nitrogen atom on an azide anion. The packing is charge-

ordered, where the cations and anions form alternating columns along all three crystallographic axes.

[C$_1$C$_1$im][NCA] crystallized in the triclinic space group P-*1* with one formula unit per asymmetric unit. The single cation-cation short contact is an edge-to-edge $\pi\cdots\pi$ interaction. Hydrogen atoms on C4 and C5 form short contacts with the terminal nitrile nitrogen and oxygen atoms of a single [NCA]$^-$ anion, which results in the shortest contact observed. C2H makes a bifurcated short contact between the central nitrogen and an oxygen atom on the same [NCA]$^-$ anion. The central nitrogen atom of the [NCA]$^-$ anion forms two short contacts with protons from the C2 and methyl positions of the same cation. The carbon atom is involved in a $\pi\cdots\pi$ interaction with a neighboring cation ring, and the terminal nitrogen atom accepts a single hydrogen bond. In comparison, the two oxygen atoms in the nitro functional group form short contacts with a total of six neighboring cation molecules. The packing consists of chains of alternating cations and anions along the *a* axis, with the anion centered over the C2 position of the cation. These chains are surrounded by antiparallel chains along *b* and *c*, forming a charge-ordered network.

[PC$_1$im][NCA] crystallized in the triclinic space group P-*1* with one formula unit per asymmetric unit. The cation-cation short contacts are present as $\pi\cdots\pi$ stacking between alkyne functional groups on unique carbon atoms and as a hydrogen bond between the methylene hydrogen atoms and two unique oxygen atoms. The acetylenic hydrogen atom makes a bifurcated short contact with O1 and O2 in the same [NCA]$^-$ anion.

The hydrogen atoms in the imidazolium ring are donated in hydrogen bonds to two unique oxygen atoms in two nitrocyanamide anions. The terminal nitrogen atom of the anion nitrile group forms three short contacts with three unique cation molecules through either C9H or C8H. In comparison, the nitro functional group in [PC$_1$im][NCA] shows more interactions, with six short contacts to five different cations observed. The oxygen atoms also form hydrogen bonds with the most acidic hydrogen atoms (the ring and acetylenic hydrogen atoms), which lead to overall stronger interactions.

The propargyl group of the cation is closely associated with the propargyl group of neighboring cations through $\pi\cdots\pi$ stacking interactions. Despite the presence of cation-cation interactions, the packing is typical salt-like. The cations and anions stack in chains along *a*. The

propargyl groups extend away from the ring cores where they can interact with each other without interfering with the charge ordering.

Differential Scanning Calorimetry (DSC). Each salt was evaluated by DSC to determine melting (T_m) and glass transitions (T_g) which are provided in **Table 1**. The six isolated solids had melting points below 100 ^{o}C: [C$_1$C$_1$im][DCA] (T_m = 22 ^{o}C), [C$_1$C$_1$im][NCA] (42 ^{o}C), [C$_1$C$_1$im][N$_3$] (43 ^{o}C with decomposition), [C$_2$C$_1$im][N$_3$] (44 ^{o}C), [PC$_1$im][NCA] (76 ^{o}C), and [C$_1$Ntri][N$_3$] (33 ^{o}C). Although 32 liquids were obtained, some caution is required since 14 of these exhibited no observable melting or glass transitions which might be a result of the hygroscopic nature observed for these compounds. Even trace amounts of water could interfere with a glass or melting transition based on previous reports of similar behavior upon the uptake of water in imidazolium-based ILs.[28] Additionally, many ILs containing the [DCA]$^-$ anion possess glass transitions below -90 ^{o}C,[2,3,29,30] which was unreachable with the experimental setup used.

Table 1. Melting (T_m) or Glass (T_g) Transitions ($^{\circ}$C).

Cation	[DCA]⁻		[NCA]⁻		[N₃]⁻	
	T_g	T_m	T_g	T_m	T_g	T_m
[C₁C₁im]⁺		22[d,e] (34)[35]		42		43[c]
[C₂C₁im]⁺	(104)[30]	-16[d] (-21)[30]	-81 (-73)[4]	18[d]		44[d]
[C₄C₁im]⁺	-83 (-90)[33]	(-6)[33]	-81 (-90)[4]		a (-74)[17]	a (26)[17]
[C₁O₂C₁im]⁺	a	a	-77 (-82)[4]		-81	14
[AC₁im]⁺	(-85)[3]		-83 (-91)[4]		a (77)[17]	a (19)[17]
[PC₁im]⁺	-74 (-61)[3]	(17)[3]		76	b	b
[C₁C₄tri]⁺	a	a	-77		-73	15[d]
[C₁Atri]⁺	a	a	-74		-75	
[C₁Ntri]⁺	-68 (-66)[3]		-67		-64	33 (43)[16]
[Pyrr₁₄]⁺	a (106)[30]	a (-55)[30]	a	a	a	a
[Pyrr₁ₐ]⁺		-21[d]	a	a	a	a
[C₄C₁py]		20	-79		a	a
[Apy]⁺	a	a	-80		a	a

[a]Due to the hygroscopic nature of this salt, no transitions were observed. [b]Compound not isolated due to side reactions. [c]Compound decomposed upon melting. [d]Values for crystallization temperatures (T_c) are included in the experimental section where observed. [e]Values for solid-solid transitions (T_{s-s}) are included in the experimental section where observed. (*Literature values in italics*).

ILs containing the [DCA]⁻ anion possessed the lowest melting points (-21 to 23 $^{\circ}$C) for a given cation of any of the anions studied here, and [DCA]⁻ salts have been previously reported to possess low viscosities and melting points due to this anion's shape and the presence of weakly coordinating nitrile functional groups.[29-36] The salts of the [NCA]⁻ anion (essentially [DCA]⁻ with one of the nitrile functional groups substituted with a more coordinating nitro group) exhibit significantly higher melting points (18 to 76 $^{\circ}$C) for a given cation. The highest melting points were observed for salts of the same cation with the much smaller [N₃]⁻ anion (14 to 44 $^{\circ}$C) with more salts with melting points above 0 $^{\circ}$C than any other anion (**Table 1**). For example, the [C₂C₁im]⁺ salts exhibited increasing melting points from -16 $^{\circ}$C for the [DCA]⁻ salt, to 18 $^{\circ}$C for the [NCA]⁻ salt, to 44 $^{\circ}$C for the [N₃]⁻ salt.

For linear alkyl derivatives of the cations, the longer the alkyl chain the lower the melting (*e.g.*, [C₁C₁im][NCA]: T_m = 42 $^{\circ}$C and [C₂C₁im][NCA]: T_m = 18 $^{\circ}$C). This trend has been

reported for other azolium ILs.[28]   Additionally, the exchange of a short alkyl chain ([C_2C_1im][NCA]: T_m = 18 $^{\circ}$C; T_g = -81 $^{\circ}$C) for an allyl functional group led to a salt with no melting transition and the depression of its glass transition ([AC_1im][NCA]: T_g = -83 $^{\circ}$C), which again matches previous IL-specific trends based on the modification of these functional groups attached to an azolium core.[28]   However, here the use of an alkyne with two degrees of unsaturation led to a dramatic rise in the observed melting point ([PC_1im][NCA]: T_m = 76 $^{\circ}$C), which might be due to the additional π stacking found in the propargyl functional group by analysis of its single-crystal structure (**Figure 2**).

Thermal Gravimetric Analyses (TGA). The $T_{5\%\,onset}$, or the temperature at which 5% of the sample has decomposed when the sample has been heated at a rate of 5 $^{\circ}$C/min to 800 $^{\circ}$C, was measured to serve as an initial indicator of a sample's overall thermal stability (**Table 2**). ILs containing the [DCA]$^-$ anion were typically the most thermally stable (for example as represented for the butylated derivatives in **Figure 4**) with $T_{5\%\,onset}$ generally increasing in the order [N_3]$^-$ < [NCA]$^-$ < [DCA]$^-$ as observed for example for the [C_4C_1im]$^+$ salts with $T_{5\%\,onset}$ = 215, 226, and 283 $^{\circ}$C, respectively (**Table 2**). This trend matches previous reports that the overall IL stability was related to the relative nucleophilicity and basicity of the anion.[37] In the case of the ILs based on the triazolium and pyridinium cations, however, $T_{5\%\,onset}$ increased from the less stable [DCA]$^-$ salts to the more stable [NCA]$^-$ salts (*e.g.*, [Apy][NCA] (199 $^{\circ}$C) *vs*. [Apy][DCA] (170 $^{\circ}$C) and [C_1Ntri][NCA] (191 $^{\circ}$C) *vs*. [C_1Ntri][DCA] (187 $^{\circ}$C)).
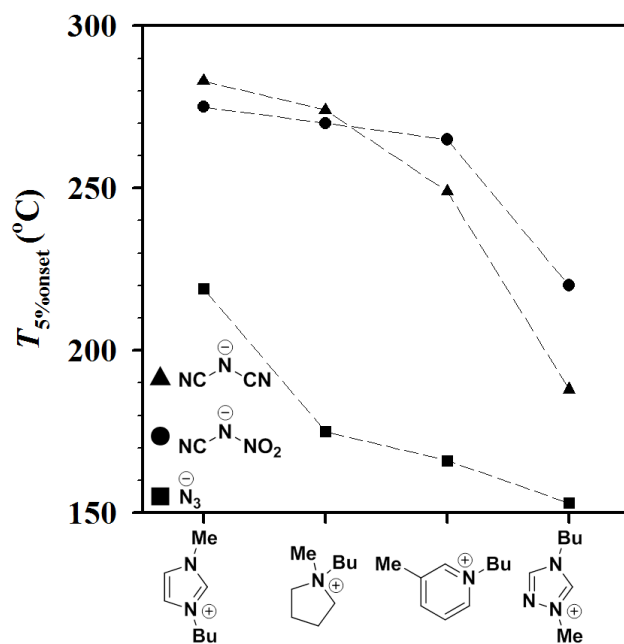
Figure 4. Five percent onset decomposition temperatures of ILs with cations that have been alkylated with a butyl functional group.

**Table 2.** Five Percent Onset of Decomposition ($T_{5\%onset}$) Temperatures (^oC)

Cation	[DCA]⁻		[NCA]⁻		[N₃]⁻	
	$T_{5\%onset}$	Literature Value	$T_{5\%onset}$	Literature Value	$T_{5\%onset}$	Literature Value
$[C_1C_1im]^+$	274	270[35]	272		216	
$[C_2C_1im]^+$	281	275[30]	274	253[4]	220	
$[C_4C_1im]^+$	283	300[33]	275	256[4]	219	
$[C_{1O2}C_1im]^+$	285		262	266[4]	226	
$[AC_1im]^+$	266	207[3]	264	220[4]	192	150[17]
$[PC_1im]^+$	197	144[3]	141		a	a
$[C_1C_4tri]^+$	188		220		153	
$[C_1Atri]^+$	172		212		129	
$[C_1Ntri]^+$	187	143[3]	196		146	129[16]
$[Pyrr_{14}]^+$	274	283[34]	270		175	
$[Pyrr_{1A}]^+$	249		258		158	
$[C_4C_1py]^+$	249		265		166	
$[Apy]^+$	170		210		110	

ᵃCompound not isolated due to side reactions.

Of the cations studied here, those based on the imidazolium core gave salts which were the most thermally stable, which matched previous comparisons of azolium and cyclic ammonium salts.[30,38] Salts prepared with pyrrolidinium and pyridinium cations were slightly less thermally stable than the imidazolium cations, but were more thermally stable than the ILs containing the 1,2,4-triazolium heterocycle which exhibited the lowest $T_{5\%onset}$ of any the cation types tested for a given functional group and anion.

The cation's substituents also greatly influenced the $T_{5\%onset}$ of the overall IL. In the case of all three anions, the thermal stability of each IL increased upon lengthening the attached alkyl chain from methyl ($[C_1C_1im][DCA]$: 274 $^{\mathrm{o}}$C) to ethyl ($[C_2C_1im][DCA]$: 281 $^{\mathrm{o}}$C) to butyl ($[C_4C_1im][DCA]$: 283 $^{\mathrm{o}}$C; **Table 2**, **Figure 5**). However, upon modification of the butyl substituent to include a single oxygen within the chain, as in $[C_{1O2}C_1im]^+$, the thermal stability trend was not as clear. In the cases of $[C_{1O2}C_1im][DCA]$ (285 $^{\mathrm{o}}$C) and $[C_{1O2}C_1im][N_3]$ (226 $^{\mathrm{o}}$C), the $T_{5\%onset}$ increased slightly relative to the respective $[C_4C_1im]^+$-ILs upon the incorporation of the oxygen atom, while in $[C_{1O2}C_1im][NCA]$ (262 $^{\mathrm{o}}$C) the onset temperature was slightly lower. The literature also reports similar conflicting trends[39] where one paper indicates that ILs containing short chain alkoxy-functionalized cations are less stable than the corresponding alkyl-functionalized ILs,[40] while other reports suggested improved thermal stability of ILs containing alkoxy-functionalized cations.[41]
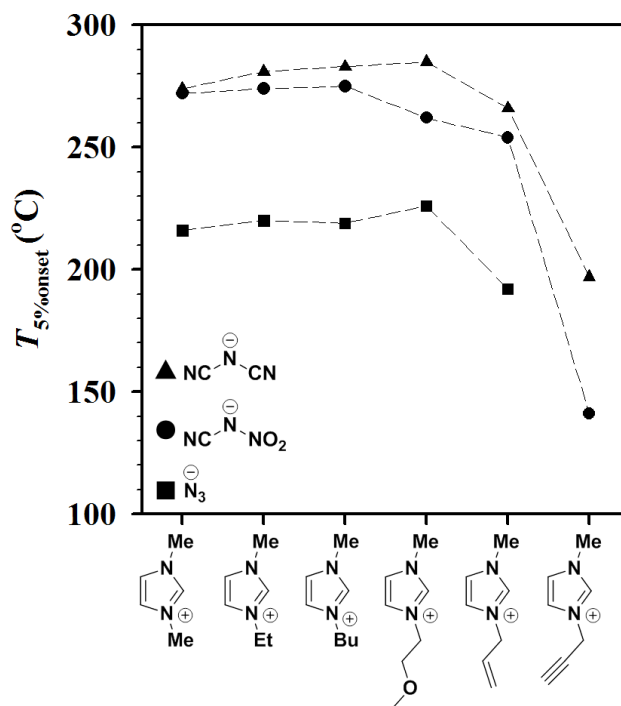
Figure 5. Onset decomposition temperatures of ILs based on an imidazolium cation paired with a [DCA]⁻, [NCA]⁻, or [N₃]⁻ anion.

Exchanging any saturated alkyl chain for one containing a single degree of unsaturation, such as in [AC₁im]⁺-ILs (**Figure 5**), led to a decrease in thermal stability with all anions, such as in [AC₁im][DCA] (266 °C) or [Pyrr₁ₐ][DCA] (249 °C) in comparison to [C₄C₁im][DCA] (283 °C) or [Pyrr₁₄][DCA] (274 °C). Additional degrees of unsaturation led to an even further decrease in thermal stability, as in [PC₁im][DCA] (197 °C).

Physical Properties of [DCA] ILs. Although salts of both the [NCA]⁻ and [DCA]⁻ anions[3-5] have been previously shown to be hypergolic (spontaneous ignition upon contact) with WFNA, we did not observe any hypergolicity with the ILs containing the [NCA]⁻ anion which were liquid at 25 °C. While crystalline samples of [PC₁im][NCA] (T_m = 76 °C) and [C₁C₁im][NCA] (T_m = 42 °C) were hypergolic with WFNA upon contact, a diminished reactivity was observed if the samples were allowed to absorb water, which suggested that the lack of hypergolicity in liquid [NCA]-based samples was due to their hygroscopic nature under the typical handing in preparation for hypergolic testing. Additionally, the [N₃]⁻ anion has been shown to only mildly react[16,17] with WFNA upon contact unless coupled with an already hypergolic ion.[42] Thus, we

chose to focus further study on the [DCA]$^-$-based ILs to find any correlation between the quantitative hypergolic ignition tests and the measured physical properties.

The viscosity of each IL containing the [DCA]$^-$ anion was determined using 1 mL of sample at 40 ^{o}C, the temperature chosen to minimize the effect of the ambient heat generated by the movement of the piston during measurement. Of the cations studied here, those based on the imidazolium core gave salts which had the lowest viscosity when the attached functional group was held constant. For example, [C$_4$C$_1$im][DCA] (19.29 cP) was reported to have the lowest viscosity of all of the ILs containing the butyl functional group, while the viscosity increased when the heterocyclic core was changed to pyridinium ([C$_4$C$_1$py][DCA] 20.20 cP), 1,2,4-triazolium (C$_1$C$_4$tri][DCA] 43.47 cP), or pyrrolidinium ([Pyrr$_{14}$][DCA] 58.45 cP). This trend matched previous comparisons of the viscosity of imidazolium and pyridinium-based ILs at 40 ^{o}C where [C$_4$C$_1$im][DCA] (16.8 cP) has been reported to possess a slightly higher viscosity than [C$_4$C$_1$py][DCA] (23.1 cP).[35,36]

The cation's substituents also greatly influenced the viscosity of the overall IL. The exchange of the butyl group (*e.g.*, [C$_4$C$_1$im][DCA] 19.28 cP) for an allyl functional group (*e.g.*, [AC$_1$im][DCA] 10.78 cP) led to a dramatic drop in viscosity for all heterocylic cores, consistent with literature reports of imidazolium salts with attached allyl functional groups possessing extremely low viscosities.[43,44] [AC$_1$im][DCA] possessed the lowest observed viscosity of any of the synthesized [DCA]$^-$-salts, (**Table 3**), however, a further increase in unsaturation index to the propargyl functionalized salt led to an increase in viscosity ([PC$_1$im][DCA] 31.68 cP).

Table 3. Physical Properties and Ignition Delays of Selected [DCA]-based ILs.

IL	Viscosity (cP)[a]	Density (g/mL)[a]	Ignition Delay (ms)[b]
[C$_2$C$_1$im][DCA]	11.30	1.103	36(5)
[C$_4$C$_1$im][DCA]	19.28 *(16.8)[36]*	1.056 *(1.053)[33]* *(1.049)[36]*	46(6) *(47)[3]*
[C$_{1O2}$C$_1$im][DCA]	21.55	1.139	51(6)
[AC$_1$im][DCA]	10.78	1.101	31(1) *(43)[3]*
[PC$_1$im][DCA]	31.68	1.159	19(0) *(15)[3]*
[C$_1$C$_4$tri][DCA]	43.47	1.110	151[c]
[C$_1$Atri][DCA]	40.17	1.166	55(7)
[C$_1$Ntri][DCA]	47.47	1.277	34(10) *(31)[3]*
[Pyrr$_{14}$][DCA]	58.45	1.046 *(1.106)[36]*	50(13) *(44)[3]*
[Pyrr$_{1A}$][DCA]	18.27	1.048	26(3)
[C$_4$C$_1$py][DCA]	20.20 *(23.1)[36]*	1.039 *(1.040)[36]*	49(0) *(37)[3]*
[Apy][DCA]	18.15	1.131	30(2)

[a]Viscosity and density measurements taken at 40 °C. [b]Ignition delay values given as an average of three hypergolic drop tests with the standard deviation of the 3 runs in parentheses. [c]Due to its highly hygroscopic nature, the sample exhibited very poor and hard to replicate ignition. *(Literature values in italics)*.

Only small differences were observed for the density of the ILs based on the heterocyclic core with the density remaining relatively constant from [C$_4$C$_1$im][DCA] (1.056 g/mL) to [Pyrr$_{14}$][DCA] (1.046 g/mL) to [C$_4$C$_1$py][DCA] (1.039 g/mL) before slightly increasing upon the modification to a 1,2,4-triazolium core as in [C$_1$C$_4$tri][DCA] (1.110 g/mL).

Much larger differences in the density of the ILs were observed based on differences in the functional group attached to each core. For example, increasing the degree of unsaturation from fully saturated ([C$_4$C$_1$im][DCA] 1.056 g/mL) to allyl functionalized ([AC$_1$im][DCA] 1.101 g/mL) to propargyl functionalized ([PC$_1$im][DCA] 1.159 g/mL) led to a direct increase in the density of the overall IL. This trend was observed with all heterocyclic cores upon the substitution of an allyl functional group for a butyl or ethyl alkyl chain. However, the highest density observed was for [C$_1$Ntri][DCA] (1.277 g/mL), which might be due to the high

percentage of N atoms and the presence of a N-N single bond, which have been previously reported to lead to ILs with higher densities.[45]

Hypergolic Tests. To prepare for the hypergolic tests, each IL containing a [DCA]⁻ anion was dried under high vacuum (~ 1×10^{-4} torr) while being stirred and heated at 70 $^{\circ}$C for between 7 and 10 days. Although all of the ILs reported have $T_{5\%onset}$ values over 70 $^{\circ}$C, special care must still be taken when heating these samples for long periods as they can decompose if heated above a certain threshold. For example, [C_1Ntri][DCA] quickly decomposed upon heating above 100 $^{\circ}$C while under vacuum, which led to visible and vigorous gas formation. After the samples had thoroughly dried, the samples were further purified through three freeze-thaw cycles to remove any entrapped gases by flash freezing the solids with liquid N_2 followed by slowly melting the sample while under reduced pressure (~1×10^{-4} torr). After this cycle was repeated, the samples were backfilled with argon and never exposed again to air until the ignition tests were conducted.

Ignition delay, or the elapsed time between contact of fuel and oxidizer and the resulting ignition, was measured through a standard hypergolic IL drop test as originally described by Schneider *et al.*[3] A single drop (10 µL) of fuel was added *via* Hamiltonian syringe to a vial containing 500 µL of WFNA. The top of the vial was vertically displaced from the bottom of the syringe by 2 cm on every drop test. The resulting ignition was monitored by a Y4 Redlake high speed camera at 1000 frames/s. Each sample was tested three times and the value for ignition delay was averaged and the standard deviation determined (**Table 3**).

Due in part to the highly sensitive nature of the hypergolic test, it is generally very difficult to compare values for ignition delay between different research groups and each slightly modified drop test apparatus. Here, we sought to provide accurate ignition delays for a number of unique IL structures provided from the same drop test set up in order to guide future computational and experimental studies. However, comparing our ignition delay values against Schneider *et al.*,[3] indicated most of the values were in good agreement, for example the ignition delay of [C_4C_1im][DCA] (46 ms) in our study compared with the literature value of 47 ms.[3] Nonetheless, in two cases ([AC_1im][DCA] and [C_4C_1py][DCA]) our experimentally determined values differed by over 10 ms, even though our results were reproducible within a standard deviation of 1 ms.

Perhaps surprisingly, the IL that had the lowest ignition delay was [PC$_1$im][DCA] with a value of only 19 ms although it had the second highest reported melting point of any of the [DCA]-based ILs (17 ^{o}C) and a moderately high viscosity (31.68 cP). This value nearly reached the 15 ms ignition delay value threshold determined for unsymmetrical dimethyl hydrazine in a similar hypergolic drop test reported in the literature.[46] Nonetheless, [C$_4$C$_1$py][DCA], which had the highest melting point (20 ^{o}C), exhibited a very poor ignition delay of 50 ms, and thus there were no discernible trends in ignition delay with respect to the melting point of the hypergolic ILs.

Although many ILs that have been reported to be hypergolic possess a low viscosity, viscosity was also not directly related to ignition delay in our data, indicating that a viscosity threshhold may be a perquisite instead of guiding modifications leading to reductions in ignition delay. There were also no correlations observed between the densities and the resulting ignition delays (see ESI†).

While the specific physical or thermal properties of the ILs did not appear to correlate with a given ignition delay change as noted above, several trends are apparent when the ignition delays are compared to the chemical structure of the IL's cation. For example, in the series of imidazolium-based ILs tested, an increasing delay was observed (**Figure 6**) with longer alkyl chains (*e.g.*, [C$_2$C$_1$im][DCA] 36 ms; [C$_4$C$_1$im][DCA] 46 ms) or the introduction of an ether functionality ([C$_{1O2}$C$_1$im][DCA] 51 ms).
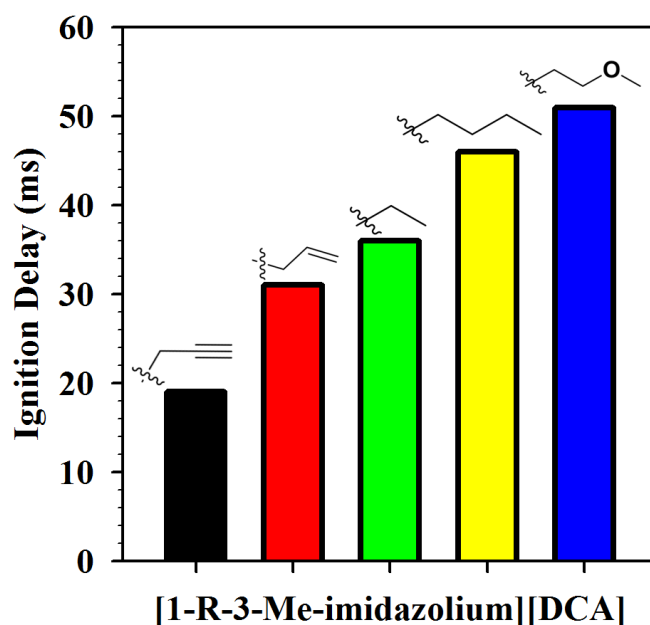
Figure 6. Ignition delay for selected [RC$_1$im][DCA] ILs.

The nature of the heterocyclic core in the cation also was important in the series of ILs tested here. For example, comparing different heterocycles with the same alkyl functional group (butyl), the ignition delay was approximately the same for the imidazolium ([C$_4$C$_1$im][DCA] 46 ms), pyridinium ([C$_4$C$_1$py][DCA] 49 ms), and pyrrolidinium ([Pyrr$_{14}$][DCA] 50 ms) ILs (**Figure 7**), but dramatically higher for the triazolium heterocycle ([C$_4$C$_1$tri][DCA] 151 ms). A similar trend was also observed when the allyl functional group was present. Here again, the ignition delays were approximately the same for pyrrolidnium ([Pyrr$_{1A}$][DCA] 26 ms), pyridinium ([Apy][DCA] 30 ms), and imidazolium ([AC$_1$im][DCA] 31 ms) ILs, with a clear increase in ignition delay observed for the related respective triazolium IL([AC$_1$tri][DCA] 55 ms). Interestingly, the N-NH$_2$ functional group in [C$_1$Ntri][DCA] led to a moderately fast ignition delay even while being attached to the least reactive heterocyclic core tested, 1,2,4-triazolium.
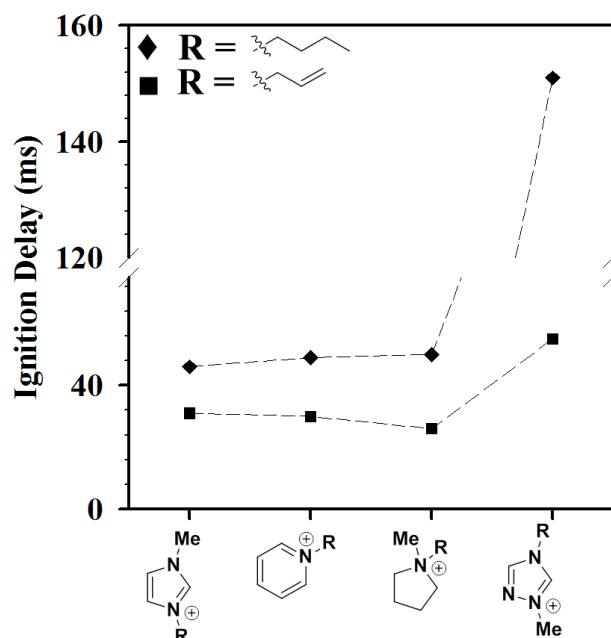
Figure 7. Ignition delay of [DCA]-based ILs with different heterocyclic cation cores which contained either a butyl or allyl functional group.

Conclusions

Overall, the only trend observed for the ignition delay was based on the attached functionality to the cation heterocycle core. Increasing unsaturation index and N-NH$_2$ functionality led to the shortest reproducible ignition delays. All allyl substituted cations (with the exception of the poorly performing [C$_1$Atri][DCA]) had ignition delays 31 ms or less. In fact, increasing the unsaturation index by another unit to incorporate an attached alkyne functional group led to the shortest reproducible ignition in this study at 19 ms for [PC$_1$im][DCA]. Incorporating N-NH$_2$ functionality led to an ignition delay of 34 ms for [C$_1$Ntri][DCA], which was the lowest reported ignition delay for any 1,2,4-triazolium-based salt.

While ignition delay is a key component to a potential hydrazine replacement system, other factors play crucial roles, such as energy density and viscosity. Even though [PC$_1$im][DCA] exhibited the shortest ignition delay, numerous other negative factors weigh against it as a potential hypergolic bipropellant replacement for hydrazine. The same functional group that promotes faster ignition (19 ms) also contributes to a higher viscosity (31.46 cP), higher melting point (17 $^{\circ}$C), and lower thermal stability (197 $^{\circ}$C). Other functional groups that also provide

short ignition delays and lower viscosities (alkene) or higher densities (N-N) should be considered further.

The development of hypergolic ILs has typically focused on the "hunt for new hypergols" or the synthetic development of new ion platforms with desired physical properties. While certain physical characteristics observed were likely prerequisites for the observation of hypergolic behavior, such as low viscosity, below a certain threshold value no reduction of ignition delay was observed by further improving these properties. Thus, a design strategy to tune the chemical nature of the cation paired with known hypergolic anions is a critical component to increase reactivity and provide lower ignition delays.

Experimental

Materials and Methods. 1-methylimidazole, 3-picoline, pyridine, 1-chlorobutane, 1-bromobutane, allyl chloride, and 1-chloro-2-methoxyethane were purchased from Sigma-Aldrich (St. Louis, MO) and used as received. Silver nitrate, sodium dicyanamide, sodium azide, 4-amino-1,2,4-triazole, *N*-methyl-pyrrolidone, iodomethane, propargyl bromide, and white fuming nitric acid were purchased from Alfa Aesar (Ward Hill, MA) and used as received. *N*-methyl-*N'*-nitro-*N*-nitrosoguanidine was purchased from TCI America (Portland, OR) and used as received. 1-Methyl-1,2,4-triazole was purchased from Matrix Scientific (Columbia, SC) and used as received. [Pyrr$_{14}$]Cl was purchased from EMD (Darmstadt, Germany) and used as received.

All Nuclear Magnetic Resonance (NMR) spectra were recorded utilizing a Bruker Avance Spectrometer Bruker/Magnex UltraShield 500 MHz (Madison, WI) or a Bruker Spectrospin DRX 360 MHz UltrashieldTM spectrometer (Madison, WI). ^{1}H (500 MHz) and ^{13}C (125 MHz) were collected using DMSO-*d6* as the solvent with TMS as the standard and shifts reported in δ (ppm). Infrared (IR) spectra were collected using a Bruker ALPHA-FTIR (Madison, WI) by direct measurement *via* attenuated total reflectance of the neat samples on a diamond crystal.

The isolated and purified ILs were dried under high vacuum (~1 × 10^{-4} torr) at 70 ^{o}C while being stirred for 7 days. The ILs were then dried through freeze-thawing with N$_{2(l)}$ while under high vacuum to remove gas trapped in the IL. This process was repeated three times to ensure the removal of trace amounts of water.

All experiments to determine thermal transitions were done on a Mettler-Toledo (Columbus, OH) Differential Scanning Calorimeter (DSC), DSC 1. The calorimeter was calibrated for temperature and cell constants using In, Zn, H_2O, and *n*-octane. Samples were weighed and sealed in aluminum pans (5–15 mg) and heated at a rate of 5 ^{o}C/min to 100 ^{o}C. Following the initial heating cycle the samples were cooled to -80 ^{o}C *via* a recirculating chiller followed by a heating cycle to 100 ^{o}C at a rate of 5 ^{o}C/min. After each dynamic temperature ramp, a 15 min isotherm was employed to ensure equilibration of the temperature in the cell. The entire cycle was repeated three times and the values for phase changes were analyzed. Each sample was referenced to an empty aluminum pan.

Thermal decompositions experiments were conducted with a Mettler-Toledo (Columbus, OH) TGA/DSC 1. The instrument's internal temperature was calibrated by observing the melting point of Au, Zn, and In. Samples of 2–15 mg were analyzed on a 70 μL alumina pan under a stream of nitrogen. Samples were heated from room temperature to 75 ^{o}C at 5 ℃/min with a 30 min isotherm at 75 ^{o}C in order to ensure excess volatiles or residual solvents were removed. Following the isotherm, samples were heated to 800 ^{o}C at 5 ^{o}C/min. The 5% onset temperature for decomposition (or $T_{5\%onset}$) was evaluated as the onset temperature where 5% of the sample had decomposed.

Viscosity measurements were taken at 40 ^{o}C with a Cambridge Viscosity (Medford, MA) Viscometer, VISCOlab 3000. Approximately 1 mL of IL was placed in the sample chamber. The correct sized piston corresponding to the expected viscosity range was added and the measurement was taken. The value for viscosity was not recorded until the error had averaged out to be less than 3%.

Density measurements were taken at 40 ^{o}C with an Anton Paar USA (Ashland, VA) density meter, DMA 500. Samples of IL (~1 mL) were inserted *via* a syringe directly into the instrument. The value for density was recorded and the sample was washed out with methanol and water.

Single Crystal X-ray Diffraction. Suitable single crystals were examined under an optical polarizing microscope, selected, and mounted on a glass fiber using silicone grease. Crystals of $[C_1NTri][N_3]$ proved to be difficult to handle under ambient conditions, rapidly absorbing water and liquefying. Coating the crystals with Paratone oil kept them viable for only a few minutes, precluding the isolation of the highest quality single crystal.

Single crystal X-ray diffraction data were measured on a Bruker diffractometer equipped with a PLATFORM goniometer and an Apex II CCD area detector (Bruker-AXS, Inc., Madison, WI) using graphite-monochromated Mo-Kα radiation. Crystals were cooled during collection under a cold nitrogen stream using an N-Helix cryostat (Oxford Cryosystems, Oxford, UK). A hemisphere of data was collected for each crystal using a strategy of omega scans with 0.5^o frame widths. Unit cell determination, data collection, data reduction, integration, absorption correction, and scaling were performed using the Apex2 software suite.[47]

The crystal structures of [C₁NTri]I, [C₁NTri][N₃], [C₁C₁im][NCA], and [PC₁im][NCA] were solved by direct methods. [C₁C₁im][N₃] was solved by locating 10 non-hydrogen atom peaks and refining the phases with dual-space recycling. All non-hydrogen atoms were refined anisotropically through full-matrix least squares refinement against F^2. Hydrogen atoms on carbon were placed in calculated positions, although difference map peaks due to hydrogen atoms were used to distinguish carbon from nitrogen in structures containing triazole rings. Hydrogen atoms on nitrogen were located from difference maps. Where possible, the coordinates of hydrogen atoms were allowed to refine freely while the thermal parameters were constrained to ride on the carrier atom. For hydrogen atoms which refined to unrealistic bond distances or angles, both the coordinates and thermal parameters were constrained to ride on the carrier atom. The coordinates of the amino hydrogen atoms in [C₁NTri][N₃] were refined to convergence using a bond distance restraint and then constrained to ride on the carrier atom at that distance.

The SHELXTL-97 software suite was used for space group determination, structure solutions by direct methods, model adjustment, and generation of ellipsoid plots.[48] SHELXS was used for solutions by direct methods, SHELXD was used for structure solution by dual space recycling and SHELXL 2013 was used for full-matrix least squares refinement.[49] Cambridge Structural Database (CSD) searches were conducted using ConQuest.[50] Short contact analyses and packing diagrams were done using the Cambridge Crystallographic Data Centre (CCDC) program Mercury.[51]

General Synthesis of Halide Precursors.[18-27] 1-methylimidazole, 1-methyl-1,2,4-triazole, 4-amino-1,2,4-triazole, *N*-methyl-pyrrolidone, 3-picoline, and pyridine were alkylated with either 1-chlorobutane, 1-bromobutane, allyl chloride, iodomethane, or 1-chloro-2-methoxyethane. In the case of reactions with 1-chlorobutane, 1-bromobutane, allyl chloride, or 1-choloro-2-

methoxyethane, a 1.1 molar excess of alkylating agent was dropwise added to a neat sample of azole at 0 ^{o}C under a constant stream of argon. The mixture was slowly brought to reflux for 24–96 h and monitored by ^{1}H NMR. In the cases of reactions of allyl chloride with 1-methyl-1,2,4-triazole, 3-picoline, and pyridine, a small amount of acetonitrile or methanol was used to dissolve the base and during the course of the reaction as the reaction either produced higher melting or hygroscopic salts. Special care was taken while handling propargyl bromide due to its high reactivity. Purchased as a stabilized solution in toluene, propargyl bromide was dropwise added to a methanolic solution of 1-methyl-imidazole at 0 ^{o}C under a constant stream of argon. The resulting solution was refluxed for 24 h and the solvents were removed *via* reduced pressure (~ 9 torr).

Synthesis of Silver Salt Precursors. **Ag[DCA].**[3] Silver dicyanamide was prepared by dropwise adding aqueous $AgNO_3$ (25 mmol, 4.247 g) into a saturated solution of equimolar sodium dicyanamide (25 mmol, 2.226 g). The resulting white solid was filtered and washed with cold methanol. The light sensitive, white solid was dried in an oven over night at 90 ^{o}C.

Ag[NCA].[4,52] *N*-methyl-*N*-nitroso-*N'*-nitro-guanidine (MNNG, 6.8 mmol, 2.00 g of 50 % w/w solution) was added piecewise to a 13.5 mL solution of NaOH (9 mmol, 0.36 g) at 0 ^{o}C over 10 min. A few drops of acetone were added to aide in dissolution, which turned bright orange. The solution was slowly warmed to room temperature. Once at 23 ^{o}C, HNO_3 (9 mmol, 0.5671 g) was added dropwise to yield a yellow solution. When the addition of HNO_3 was completed a saturated solution of $AgNO_3$ (6.8 mmol, 1.155 g) was added dropwise. A white solid immediately precipitated. The resulting mixture was stirred at room temperature for 30 min. The solution with freshly precipitated Ag[NCA] was cooled to 0 ^{o}C in a freezer and the resulting solid was filtered. Special care was taken to wash the solid with water and methanol without allowing the solid to completely dry.

Ag[N$_3$].[16,17] A solution of sodium azide (25 mmol, 1.625 g) was dissolved into the minimum amount of water. A solution of silver nitrate (25 mmol, 4.247 g) was dropwise added to precipitate silver azide. The excess water was decanted and replaced gradually with methanol. Methanol was decanted 3 more times in the same fashion to fully replace water with methanol. $Ag[N_3]$ was kept as a dispersion in methanol due to concerns about the sensitivity of the dry $Ag[N_3]$ powder.

Metathesis Reactions. **[DCA]⁻-Based ILs.**[3] A suspension of silver dicyanamide (22 mmol, 3.826 g) was prepared in 25 mL of methanol. The halide salt (20 mmol) was dissolved in methanol and dropwise added to the suspension of silver dicyanamide and the reaction was covered with aluminum foil to prevent light oxidation. The reaction was stirred at room temperature for at least 3 days and the excess silver dicyanamide and resulting silver halide salt were filtered off. The targeted dicyanamide IL was purified through solvent evaporation via reduced pressure.

[NCA]⁻-Based ILs.[4] A methanol solution (approximately 1 mmol/mL) of azolium halide (5 mmol) was dropwise added to the suspension of silver nitrocyanamide in methanol. The reaction was covered with aluminum foil and allowed to stir for 3 days to ensure metathesis completion. The remaining silver salt starting material and resulting silver halide were removed by vacuum filtration. The newly synthesized nitrocyanamide ILs were purified by salting out of methanol with diethyl ether.

[N₃]⁻-Based ILs.[16,17] A methanol solution (approximately 1 mmol/mL) of azolium halide (20 mmol) was dropwise added to the suspension of silver azide (22 mmol) in methanol. The reaction was stirred overnight and covered with aluminum foil to prevent light oxidation. The product was isolated by removing the excess silver azide and generated silver halide by filtration. The targeted azide IL was purified through solvent evaporation *via* reduced pressure.

1,3-dimethyl-imidazolium dicyanamide ([C₁C₁im][DCA]). ^{1}H NMR (500 MHz, DMSO-*d6*) δ ppm: 9.02 (s, 1H, C2-H), 7.68 (s, 1H, C4/5-H), 7.67 (s, 1H, C4/5-H), 3.85 (s, 6H, N-CH3); ^{13}C NMR (125 MHz, DMSO-*d6*) δ ppm: 137.5 (s), 123.8 (s), 119.5 (s), 36.1 (s). TGA: $T_{5\% \text{ onset}} = 274$ °C. DSC: $T_c = 41$ °C, $T_m = 22$ °,C $T_{s-s} = -7$ °C.

1,3-dimethyl-imidazolium nitrocyanamide ([C₁C₁im][NCA]). ^{1}H NMR (500 MHz, *DMSO-d6*) δ ppm: 9.02 (s, 1H, C2-H), 7.67 (s, 1H, C4/5-H), 7.66 (s, 1H, C4/5-H), 3.85 (s, 6H, N-CH₃); ^{13}C NMR (125 MHz, DMSO-*d6*) δ ppm: 137.6 (s), 124.1 (s), 117.2 (s), 36.4 (s). TGA: $T_{5\% \text{ onset}} = 272$ °C. DSC: $T_m = 42$ °C. Single crystals were obtained after slowly cooling a molten sample to 25 °C.

1,3-dimethyl-imidazolium azide ([C₁C₁im][N₃]). ^{1}H NMR (500 MHz, *DMSO-d6*) δ ppm: 9.08 (s, 1H, C2-H), 7.70 (s, 1H, C4/5-H), 7.69 (s, 1H, C4/5-H), 3.86 (s, 6H, N-CH₃); ^{13}C NMR (125 MHz, *DMSO-d6*) δ ppm: 137.7 (s), 124.1 (s), 36.2 (s). TGA: $T_{5\% \text{ onset}} = 216$ °C. DSC: $T_m = $

43 ^{o}C (decomposition on melting).   Single crystals were obtained after slowly evaporating methanol at 25 ^{o}C.

1-ethyl-3-methyl-imidazolium dicyanamide ([C$_2$C$_1$im][DCA]).   ^{1}H NMR (500 MHz, *DMSO-d6*) δ ppm: 9.11 (s, 1H, C2-H), 7.78 (s, 1H, C4/5-H), 7.70 (s, 1H, C4/5-H), 4.20 (q, 2H, N-C$\underline{H}_2$-CH$_3$), 3.85 (s, 3H, N-CH$_3$), 1.42 (t, 3H, N-CH$_2$-C$\underline{H}_3$); ^{13}C NMR (125 MHz, DMSO-*d6*) δ ppm: 136.1 (s, C2), 123.5 (s, C4/5), 121.9 (s, C4/5), 119.0 (s, N-C≡N), 44.0 (s, N-$\underline{C}$H$_2$-CH$_3$), 35.6 (s, N-CH$_3$), 15.0 (s, N-CH$_2$-$\underline{C}$H$_3$). TGA: $T_{5\% \text{ onset}}$ = 281 ^{o}C. DSC: T_m = -16 ^{o}C, T_c = -45 ^{o}C.

1-ethyl-3-methyl-imidazolium nitrocyanamide ([C$_2$C$_1$im][NCA]).   ^{1}H NMR (500 MHz, *DMSO-d6*) δ ppm: 9.09 (s, 1H, C2-H), 7.75 (s, 1H, C4/5-H), 7.67 (s, 1H, C4/5-H), 4.20 (q, 2H, N-C$\underline{H}_2$-CH$_3$), 3.85 (s, 3H, N-CH$_3$), 1.42 (t, 3H, N-CH$_2$-C$\underline{H}_3$); ^{13}C NMR (125 MHz, DMSO-*d6*) δ ppm: 136.7 (s, C2), 124.0 (s, C4/5), 122.4 (s, C4/5), 117.3 (s, O$_2$N-N-C≡N), 44.6 (s, N-$\underline{C}$H$_2$-CH$_3$), 36.1 (s, N-CH$_3$), 15.3 (s, N-CH$_2$-$\underline{C}$H$_3$). TGA: $T_{5\% \text{ onset}}$ = 274 ^{o}C. DSC: T_g = -81 ^{o}C, T$_c$ on heating = -49 ^{o}C, T_m = 18 ^{o}C, T_c on cooling = -28 ^{o}C.

1-ethyl-3-methyl-imidazolium azide ([C$_2$C$_1$im][N$_3$]).   ^{1}H NMR (500 MHz, *DMSO-d6*) δ ppm: 9.14 (s, 1H, C2-H), 7.80 (s, 1H, C4/5-H), 7.71 (s, 1H, C4/5-H), 4.20 (q, 2H, N-C$\underline{H}_2$-CH$_3$), 3.85 (s, 3H, N-CH$_3$), 1.40 (t, 3H, N-CH$_2$-C$\underline{H}_3$); ^{13}C NMR (125 MHz, DMSO-*d6*) δ ppm: 136.7 (s, C2), 124.0 (s, C4/5), 122.4 (s, C4/5), 44.6 (s, N-$\underline{C}$H$_2$-CH$_3$), 36.1 (s, N-CH$_3$), 15.6 (s, N-CH$_2$-$\underline{C}$H$_3$). TGA: $T_{5\% \text{ onset}}$ = 220 ^{o}C. DSC: T_m = 44 ^{o}C, T_c = -7 ^{o}C.

1-butyl-3-methyl-imidazolium dicyanamide ([C$_4$C$_1$im][DCA]).   ^{1}H NMR (500 MHz, *DMSO-d6*) δ ppm: 9.11 (s, 1H, C2-H), 7.76 (s, 1H, C4/5-H), 7.70 (s, 1H, C4/5-H), 4.16 (t, 2H, N-C$\underline{H}_2$-CH$_2$-CH$_2$-CH$_3$), 3.85 (s, 3H, N-CH$_3$), 1.76 (quintet, 2H, N-CH$_2$-C$\underline{H}_2$-CH$_2$-CH$_3$), 1.24 (sextet, 2H, N-CH$_2$-CH$_2$-C$\underline{H}_2$-CH$_3$), 0.90 (t, 3H, N-CH$_2$-CH$_2$-CH$_2$-C$\underline{H}_3$); ^{13}C NMR (125 MHz, DMSO-*d6*) δ ppm: 136.4 (s, C2), 123.5 (s, C4/5), 122.1 (s, C4/5), 119.0 (s, N-C≡N), 48.4 (s, N-$\underline{C}$H$_2$-CH$_2$-CH$_2$-CH$_3$), 35.6 (s, N-CH$_3$), 31.2 (s, N-CH$_2$-$\underline{C}$H$_2$-CH$_2$-CH$_3$), 18.6 (s, N-CH$_2$-CH$_2$-$\underline{C}$H$_2$-CH$_3$), 13.1 (s, N-CH$_2$-CH$_2$-CH$_2$-$\underline{C}$H$_3$). TGA: $T_{5\% \text{ onset}}$ = 283 ^{o}C. DSC: No thermal transitions were observed in the targeted range.

1-butyl-3-methyl-imidazolium nitrocyanamide ([C$_4$C$_1$im][NCA]).   ^{1}H NMR (500 MHz, *DMSO-d6*) δ ppm: 9.10 (s, 1H, C2-H), 7.75 (s, 1H, C4/5-H), 7.69 (s, 1H, C4/5-H), 4.16 (t, 2H, N-C$\underline{H}_2$-CH$_2$-CH$_2$-CH$_3$), 3.85 (s, 3H, N-CH$_3$), 1.77 (quintet, 2H, N-CH$_2$-C$\underline{H}_2$-CH$_2$-CH$_3$), 1.27 (sextet, 2H, N-CH$_2$-CH$_2$-C$\underline{H}_2$-CH$_3$), 0.90 (t, 3H, N-CH$_2$-CH$_2$-CH$_2$-C$\underline{H}_3$); ^{13}C NMR (125 MHz, DMSO-*d6*) δ ppm: 137.0 (s, C2), 124.1 (s, C4/5), 122.7 (s, C4/5), 117.3 (s, O$_2$N-N-C≡N), 49.0

(s, N-C<u>H</u>₂-CH₂-CH₂-CH₃), 36.2 (s, N-CH₃), 31.8 (s, N-CH₂-C<u>H</u>₂-CH₂-CH₃), 19.2 (s, N-CH₂-CH₂-C<u>H</u>₂-CH₃), 13.7 (s, N-CH₂-CH₂-CH₂-C<u>H</u>₃). TGA: $T_{5\% \text{ onset}}$ = 275 °C. DSC: T_g = -81 °C.

1-butyl-3-methyl-imidazolium azide ([C₄C₁im][N₃]). ¹H NMR (500 MHz, *DMSO-d6*) δ ppm: 9.21 (s, 1H, C2-H), 7.81 (s, 1H, C4/5-H), 7.73 (s, 1H, C4/5-H), 4.17 (t, 2H, N-C<u>H</u>₂-CH₂-CH₂-CH₃), 3.86 (s, 3H, N-CH₃), 1.76 (quintet, 2H, N-CH₂-C<u>H</u>₂-CH₂-CH₃), 1.24 (sextet, 2H, N-CH₂-CH₂-C<u>H</u>₂-CH₃), 0.87 (t, 3H, N-CH₂-CH₂-CH₂-C<u>H</u>₃); ¹³C NMR (125 MHz, DMSO-*d6*) δ ppm: 137.1 (s, C2), 124.1 (s, C4/5), 122.8 (s, C4/5), 49.0 (s, N-C<u>H</u>₂-CH₂-CH₂-CH₃), 36.1 (s, N-CH₃), 31.8 (s, N-CH₂-C<u>H</u>₂-CH₂-CH₃), 19.2 (s, N-CH₂-CH₂-C<u>H</u>₂-CH₃), 13.7 (s, N-CH₂-CH₂-CH₂-C<u>H</u>₃). TGA: $T_{5\% \text{ onset}}$ = 219 °C. DSC: No thermal transitions were observed in the targeted range.

1-(2-methoxyethyl)-3-methyl-imidazolium dicyanamide ([C₁O₂C₁im][DCA]). ¹H NMR (500 MHz, *DMSO-d6*) δ ppm: 9.08 (s, 1H, C2-H), 7.73 (s, 1H, C4/5-H), 7.69 (s, 1H, C4/5-H), 4.35 (t, 2H, N-C<u>H</u>₂-CH₂-O-CH₃), 3.87 (s, 3H, N-CH₃), 3.68 (t, 2H, N-CH₂-C<u>H</u>₂-O-CH₃), 3.27 (s, 3H, N-CH₂-CH₂-O-C<u>H</u>₃); ¹³C NMR (125 MHz, DMSO-*d6*) δ ppm: 136.7 (s, C2), 123.4 (s, C4/5), 122.5 (s, C4/5), 119.3 (s, N-C≡N), 69.5 (s, N-CH₂-C<u>H</u>₂-O-CH₃), 58.0 (s, N-CH₂-CH₂-O-C<u>H</u>₃), 48.6 (s, N-C<u>H</u>₂-CH₂-O-CH₃), 35.7 (s, N-CH₃). TGA: $T_{5\% \text{ onset}}$ = 285 °C. DSC: T_g = -85 °C.

1-(2-methoxyethyl)-3-methyl-imidazolium nitrocyanamide ([C₁O₂C₁im][NCA]). ¹H NMR (500 MHz, *DMSO-d6*) δ ppm: 9.07 (s, 1H, C2-H), 7.71 (s, 1H, C4/5-H), 7.68 (s, 1H, C4/5-H), 4.35 (t, 2H, N-C<u>H</u>₂-CH₂-O-CH₃), 3.87 (s, 3H, N-CH₃), 3.68 (t, 2H, N-CH₂-C<u>H</u>₂-O-CH₃), 3.26 (s, 3H, N-CH₂-CH₂-O-C<u>H</u>₃); ¹³C NMR (125 MHz, DMSO-*d6*) δ ppm: 137.2 (s, C2), 123.9 (s, C4/5), 123.0 (s, C4/5), 117.2 (s, N-C≡N), 70.0 (s, N-CH₂-C<u>H</u>₂-O-CH₃), 58.5 (s, N-CH₂-CH₂-O-C<u>H</u>₃), 49.1 (s, N-C<u>H</u>₂-CH₂-O-CH₃), 36.2 (s, N-CH₃). TGA: $T_{5\% \text{ onset}}$ = 262 °C. DSC: T_g = -77 °C.

1-(2-methoxyethyl)-3-methyl-imidazolium azide ([C₁O₂C₁im][N₃]). ¹H NMR (500 MHz, *DMSO-d6*) δ ppm: 9.15 (s, 1H, C2-H), 7.76 (s, 1H, C4/5-H), 7.72 (s, 1H, C4/5-H), 4.37 (t, 2H, N-C<u>H</u>₂-CH₂-O-CH₃), 3.87 (s, 3H, N-CH₃), 3.69 (t, 2H, N-CH₂-C<u>H</u>₂-O-CH₃), 3.27 (s, 3H, N-CH₂-CH₂-O-C<u>H</u>₃); ¹³C NMR (125 MHz, DMSO-*d6*) δ ppm: 137.4 (s, C2), 123.9 (s, C4/5), 123.1 (s, C4/5), 70.0 (s, N-CH₂-C<u>H</u>₂-O-CH₃), 58.5 (s, N-CH₂-CH₂-O-C<u>H</u>₃), 49.1 (s, N-C<u>H</u>₂-CH₂-O-CH₃), 36.1 (s, N-CH₃). TGA: $T_{5\% \text{ onset}}$ = 226 °C. DSC: T_g = -81 °C, T_c = -15 °C, T_m = 14 °C.

1-allyl-3-methyl-imidazolium dicyanamide ([AC₁im][DCA]). ¹H NMR (500 MHz, *DMSO-d6*) δ ppm: 9.10 (s, 1H, C2-H), 7.73 (s, 1H, C4/5-H), 7.71 (s, 1H, C4/5-H), 6.04 (ddt, 1H,

CH_2-C$\underline{H}$=CH_2), 5.37 (dd, 1H, =CH_2 *cis* to C-H), 5.30 (dd, 1H, =CH_2 *trans* to C-H), 4.85 (d, 2H, N-C$\underline{H}_2$-CH=CH_2), 3.87 (s, 3H, N-CH_3); ^{13}C NMR (125 MHz, DMSO-*d6*) δ ppm: 137.1 (s, C2), 132.2 (s, -$\underline{C}$H=CH_2), 124.2 (s, C4/5), 122.8 (s, C4/5), 120.6 (s, -CH=$\underline{C}H_2$), 119.6 (s, N-C≡N), 51.3 (s, N-$\underline{C}H_2$-CH=CH_2), 36.3 (s, N-CH_3). TGA: $T_{5\% \text{ onset}}$ = 266 $^{\circ}$C. DSC: No thermal transitions were observed in the targeted range.

1-allyl-3-methyl-imidazolium nitrocyanamide ([AC$_1$im][NCA]). ^{1}H NMR (500 MHz, *DMSO-d6*) δ ppm: 9.09 (s, 1H, C2-H), 7.71 (s, 1H, C4/5-H), 7.69 (s, 1H, C4/5-H), 6.03 (ddt, 1H, CH_2-C$\underline{H}$=CH_2), 5.37 (dd, 1H, =CH_2 *cis* to C-H), 5.30 (dd, 1H, =CH_2 *trans* to C-H), 4.84 (d, 2H, N-C$\underline{H}_2$-CH=CH_2), 3.87 (s, 3H, N-CH_3); ^{13}C NMR (125 MHz, DMSO-*d6*) δ ppm: 137.1 (s, C2), 132.1 (s, -$\underline{C}$H=CH_2), 124.2 (s, C4/5), 122.8 (s, C4/5), 120.7 (s, -CH=$\underline{C}H_2$), 117.3 (s, O_2N-N-C≡N), 51.3 (s, N-$\underline{C}H_2$-CH=CH_2), 36.3 (s, N-CH_3). TGA: $T_{5\% \text{ onset}}$ = 264 $^{\circ}$C. DSC: T_g = -83 $^{\circ}$C.

1-allyl-3-methyl-imidazolium azide ([AC$_1$im][N$_3$]). ^{1}H NMR (500 MHz, *DMSO-d6*) δ ppm: 9.18 (s, 1H, C2-H), 7.75 (s, 1H, C4/5-H), 7.74 (s, 1H, C4/5-H), 6.03 (ddt, 1H, CH_2-C$\underline{H}$=CH_2), 5.34 (dd, 1H, =CH_2 *cis* to C-H), 5.31 (dd, 1H, =CH_2 *trans* to C-H), 4.86 (d, 2H, N-C$\underline{H}_2$-CH=CH_2), 3.88 (s, 3H, N-CH_3); ^{13}C NMR (125 MHz, DMSO-*d6*) δ ppm: 137.2 (s, C2), 132.2 (s, -$\underline{C}$H=CH_2), 124.2 (s, C4/5), 122.8 (s, C4/5), 120.7 (s, -CH=$\underline{C}H_2$), 51.2 (s, N-$\underline{C}H_2$-CH=CH_2), 36.3 (s, N-CH_3). TGA: $T_{5\% \text{ onset}}$ = 192 $^{\circ}$C. DSC: No thermal transitions were observed in the targeted range.

1-propargyl-3-methyl-imidazolium dicyanamide ([PC$_1$im][DCA]). ^{1}H NMR (500 MHz, *DMSO-d6*) δ ppm: 9.20 (s, 1H, C2-H), 7.79 (s, 1H, C4/5-H), 7.75 (s, 1H, C4/5-H), 5.20 (d, 2H, N-CH_2-C≡C), 3.88 (s, 3H, N-CH_3), 3.84 (t, 1H, C≡CH); ^{13}C NMR (125 MHz, DMSO-*d6*) δ ppm: 136.5 (s, C2), 124.0 (s, C4/5), 122.0 (s, C4/5), 199.0 (s, N-C≡N), 78.8 (s, ≡CH), 76.0 (-C≡), 38.4 (s, N-CH_2-Alkyne), 35.9 (s, N-CH_3). TGA: $T_{5\% \text{ onset}}$ = 197 $^{\circ}$C. DSC: T_g = -74 $^{\circ}$C.

1-propargyl-3-methyl-imidazolium nitrocyanamide ([PC$_1$im][NCA]). ^{1}H NMR (500 MHz, *DMSO-d6*) δ ppm: 9.22 (s, 1H, C2-H), 7.82 (s, 1H, C4/5-H), 7.64 (s, 1H, C4/5-H), 5.21 (d, 2H, N-CH_2-C≡C), 3.88 (s, 3H, N-CH_3), 3.85 (t, 1H, C≡CH); ^{13}C NMR (125 MHz, DMSO-*d6*) δ ppm: 136.0 (s, C2), 124.5 (s, C4/5), 122.6 (s, C4/5), 119.5 (s, O_2N-N-C≡N), 79.4 (s, ≡CH), 76.6 (-C≡), 39.0 (s, N-CH_2-Alkyne), 36.4 (s, N-CH_3). TGA: $T_{5\% \text{ onset}}$ = 141 $^{\circ}$C. DSC: T_c = -10 $^{\circ}$C, T_m = 76 $^{\circ}$C. Single crystals were obtained after slowly cooling a molten sample to 25 $^{\circ}$C.

1-methyl-4-butyl-1,2,4-triazolium dicyanamide ([C$_1$C$_4$tri][DCA]). ^{1}H NMR (500 MHz, *DMSO-d6*) δ ppm: 10.05 (s, 1H, C3-H), 9.20 (s, 1H, C5-H), 4.24 (t, 2H, N-C$\underline{H}_2$-CH_2-CH_2-CH_3),

4.06 (s, 3H, N-CH$_3$), 1.80 (quintet, 2H, N-CH$_2$-C$\underline{\text{H}}_2$-CH$_2$-CH$_3$), 1.30 (sextet, 2H, N-CH$_2$-CH$_2$-C$\underline{\text{H}}_2$-CH$_3$), 0.91 (t, 3H, N-CH$_2$-CH$_2$-CH$_2$-C$\underline{\text{H}}_3$); ^{13}C NMR (125 MHz, DMSO-*d6*) δ ppm: 145.0 (s, C3), 142.4 (s, C5), 119.4 (s, N-C≡N), 47.5 (s, N-C$\underline{\text{H}}_2$-CH$_2$-CH$_2$-CH$_3$), 39.1 (s, N-CH$_3$), 31.3 (s, N-CH$_2$-C$\underline{\text{H}}_2$-CH$_2$-CH$_3$), 19.2 (s, N-CH$_2$-CH$_2$-C$\underline{\text{H}}_2$-CH$_3$), 13.7 (s, N-CH$_2$-CH$_2$-CH$_2$-C$\underline{\text{H}}_3$). TGA: $T_{5\% \text{ onset}}$ = 188 $^{\text{o}}$C. DSC: No thermal transitions were observed in the targeted range.

1-methyl-4-butyl-1,2,4-triazolium nitrocyanamide ([C$_1$C$_4$tri][NCA]). ^{1}H NMR (500 MHz, *DMSO-d6*) δ ppm: 10.05 (s, 1H, C3-H), 9.20 (s, 1H, C5-H), 4.24 (t, 2H, N-C$\underline{\text{H}}_2$-CH$_2$-CH$_2$-CH$_3$), 4.06 (s, 3H, N-CH$_3$), 1.80 (quintet, 2H, N-CH$_2$-C$\underline{\text{H}}_2$-CH$_2$-CH$_3$), 1.30 (sextet, 2H, N-CH$_2$-CH$_2$-C$\underline{\text{H}}_2$-CH$_3$), 0.91 (t, 3H, N-CH$_2$-CH$_2$-CH$_2$-C$\underline{\text{H}}_3$); ^{13}C NMR (125 MHz, DMSO-*d6*) δ ppm: 145.0 (s, C3), 143.3 (s, C5), 117.2 (s, N-C≡N), 47.6 (s, N-C$\underline{\text{H}}_2$-CH$_2$-CH$_2$-CH$_3$), 39.1 (s, N-CH$_3$), 31.3 (s, N-CH$_2$-C$\underline{\text{H}}_2$-CH$_2$-CH$_3$), 19.2 (s, N-CH$_2$-CH$_2$-C$\underline{\text{H}}_2$-CH$_3$), 13.7 (s, N-CH$_2$-CH$_2$-CH$_2$-C$\underline{\text{H}}_3$). TGA: $T_{5\% \text{ onset}}$ = 220 $^{\text{o}}$C. DSC: T_g = -77 $^{\text{o}}$C .

1-methyl-4-butyl-1,2,4-triazolium azide ([C$_1$C$_4$tri][N$_3$]). ^{1}H NMR (500 MHz, *DMSO-d6*) δ ppm: 10.11 (s, 1H, C3-H), 9.23 (s, 1H, C5-H), 4.26 (t, 2H, N-C$\underline{\text{H}}_2$-CH$_2$-CH$_2$-CH$_3$), 4.07 (s, 3H, N-CH$_3$), 1.81 (quintet, 2H, N-CH$_2$-C$\underline{\text{H}}_2$-CH$_2$-CH$_3$), 1.30 (sextet, 2H, N-CH$_2$-CH$_2$-C$\underline{\text{H}}_2$-CH$_3$), 0.92 (t, 3H, N-CH$_2$-CH$_2$-CH$_2$-C$\underline{\text{H}}_3$); ^{13}C NMR (125 MHz, DMSO-*d6*) δ ppm: 145.0 (s, C3), 143.4 (s, C5), 47.6 (s, N-C$\underline{\text{H}}_2$-CH$_2$-CH$_2$-CH$_3$), 39.1 (s, N-CH$_3$), 31.3 (s, N-CH$_2$-C$\underline{\text{H}}_2$-CH$_2$-CH$_3$), 19.2 (s, N-CH$_2$-CH$_2$-C$\underline{\text{H}}_2$-CH$_3$), 13.7 (s, N-CH$_2$-CH$_2$-CH$_2$-C$\underline{\text{H}}_3$). TGA: $T_{5\% \text{ onset}}$ = 153 $^{\text{o}}$C. DSC: T_g = -73 $^{\text{o}}$C, T_c on heat = -27 $^{\text{o}}$C, T_c on cool, -19 $^{\text{o}}$C, T_m = 15 $^{\text{o}}$C.

1-methyl-4-allyl-1,2,4-triazolium dicyanamide ([C$_1$Atri][DCA]). ^{1}H NMR (500 MHz, *DMSO-d6*) δ ppm: 10.06 (s, 1H, C3-H), 9.19 (s, 1H, C5-H), 6.06 (ddt, 1H, CH$_2$-C$\underline{\text{H}}$=CH$_2$), 5.42 (dd, 1H, =CH$_2$ *cis* to C-H), 5.38 (dd, 1H, =CH$_2$ *trans* to C-H), 4.93 (d, 2H, N-C$\underline{\text{H}}_2$-CH=CH$_2$), 4.08 (s, 3H, N-CH$_3$); ^{13}C NMR (125 MHz, DMSO-*d6*) δ ppm: 151.8 (s, C3), 145.0 (s, C5), 131.1 (s, -C$\underline{\text{H}}$=CH$_2$), 121.6 (s, -CH=C$\underline{\text{H}}_2$), 119.5 (s, N-C≡N), 49.8 (s, N-C$\underline{\text{H}}_2$-CH=CH$_2$), 36.1 (s, N-CH$_3$). TGA: $T_{5\% \text{ onset}}$ = 172 $^{\text{o}}$C. DSC: No thermal transitions were observed in the targeted range.

1-methyl-4-allyl-1,2,4-triazolium azide ([C$_1$Atri][N$_3$]). ^{1}H NMR (500 MHz, *DMSO-d6*) δ ppm: 10.08 (s, 1H, C3-H), 9.20 (s, 1H, C5-H), 6.06 (ddt, 1H, CH$_2$-C$\underline{\text{H}}$=CH$_2$), 5.43 (dd, 1H, =CH$_2$ *cis* to C-H), 5.40 (dd, 1H, =CH$_2$ *trans* to C-H), 4.94 (d, 2H, N-C$\underline{\text{H}}_2$-CH=CH$_2$), 4.08 (s, 3H, N-CH$_3$); ^{13}C NMR (125 MHz, DMSO-*d6*) δ ppm: 151.8 (s, C3), 145.0 (s, C5), 131.2 (s, -

C̲H=CH$_2$), 121.6 (s, -CH=C̲H$_2$), 119.5 (s, N-C≡N), 49.8 (s, N-C̲H$_2$-CH=CH$_2$), 36.1 (s, N-C̲H$_3$). TGA: $T_{5\% \text{ onset}}$ = 129 °C. DSC: T_g = -75 °C .

1-methyl-4-allyl-1,2,4-triazolium nitrocyanamide ([C$_1$Atri][NCA]). ^{1}H NMR (500 MHz, *DMSO-d6*) δ ppm: 10.05 (s, 1H, C3-H), 9.18 (s, 1H, C5-H), 6.06 (ddt, 1H, CH$_2$-C̲H=CH$_2$), 5.43 (dd, 1H, =CH$_2$ *cis* to C-H), 5.40 (dd, 1H, =CH$_2$ *trans* to C-H), 4.93 (d, 2H, N-C̲H$_2$-CH=CH$_2$), 4.08 (s, 3H, N-CH$_3$); ^{13}C NMR (125 MHz, DMSO-*d6*) δ ppm: 151.8 (s, C3), 145.0 (s, C5), 131.2 (s, -C̲H=CH$_2$), 121.6 (s, -CH=C̲H$_2$), 117.2 (s, O$_2$N-N-C≡N), 49.3 (s, N-C̲H$_2$-CH=CH$_2$), 36.2 (s, N-CH$_3$). TGA: $T_{5\% \text{ onset}}$ = 212 °C. DSC: T_g = -74 °C.

1-methyl-4-amino-1,2,4-triazolium dicyanamide ([C$_1$Ntri][DCA]). ^{1}H NMR (500 MHz, *DMSO-d6*) δ ppm: 10.07 (s, 1H, C3-H), 9.15 (s, 1H, C5-H), 6.95 (s, 2H, N-NH̲$_2$), 4.03 (s, 3H, N-CH$_3$); ^{13}C NMR (125 MHz, DMSO-*d6*) δ ppm: 144.5 (s, C3), 142.4 (s, C5), 118.6 (s, N-C≡N), 38.4 (s, N-CH$_3$). TGA: $T_{5\% \text{ onset}}$ = 187 °C. DSC: T_g = -68 °C.

1-methyl-4-amino-1,2,4-triazolium nitrocyanamide ([C$_1$Ntri][NCA]). ^{1}H NMR (500 MHz, *DMSO-d6*) δ ppm: 10.07 (s, 1H, C3-H), 9.15 (s, 1H, C5-H), 6.96 (s, 2H, N-NH̲$_2$), 4.04 (s, 3H, N-CH$_3$); ^{13}C NMR (125 MHz, DMSO-*d6*) δ ppm: 145.5 (s, C3), 143.3 (s, C5), 117.2 (O$_2$N-N-C≡N), 39.3 (s, N-CH$_3$). TGA: $T_{5\% \text{ onset}}$ = 196 °C. DSC: T_g = -67 °C.

1-methyl-4-amino-1,2,4-triazolium azide ([C$_1$Ntri][N$_3$]). ^{1}H NMR (500 MHz, *DMSO-d6*) δ ppm: 10.14 (s, 1H, C3-H), 9.12 (s, 1H, C5-H), 7.11 (s, 2H, N-NH̲$_2$), 4.04 (s, 3H, N-CH$_3$); ^{13}C NMR (125 MHz, DMSO-*d6*) δ ppm: 144.5 (s, C3), 143.4 (s, C5), 39.3 (s, N-CH$_3$). TGA: $T_{5\% \text{ onset}}$ = 146 °C. DSC: T_g = -64 °C, T_m = 33 °C. Single crystals were obtained after slowly cooling a molten sample to 25 °C.

N-butyl-N-methyl-pyrrolidinium dicyanamide ([Pyrr$_{14}$][DCA]). ^{1}H NMR (500 MHz, *DMSO-d6*) δ ppm: 3.44 (m, 4H, -C̲H$_2$-N-C̲H$_2$-), 3.30 (m, 2H, N-C̲H$_2$-CH$_2$-CH$_2$-CH$_3$), 2.98 (s, 3H, N-CH$_3$), 2.08 (m, 4H, -C̲H$_2$-C̲H$_2$-), 1.68 (quintet, 2H, N-CH$_2$-C̲H$_2$-CH$_2$-CH$_3$), 1.32 (sextet, 2H, N-CH$_2$-CH$_2$-C̲H$_2$-CH$_3$), 0.94 (t, 3H, N-CH$_2$-CH$_2$-CH$_2$-C̲H$_3$); ^{13}C NMR (125 MHz, DMSO-*d6*) δ ppm: 119.6 (s, N-C≡N), 63.90 (s, C̲H$_2$-N-C̲H$_2$-), 63.4 (N-C̲H$_2$-CH$_2$-CH$_2$-CH$_3$), 48.0 (s, N-CH$_3$), 25.4 (N-CH$_2$-C̲H$_2$-CH$_2$-CH$_3$), 21.6 (s, -C̲H$_2$-C̲H$_2$-), 19.8 (s, N-CH$_2$-CH$_2$-C̲H$_2$-CH$_3$), 13.9 (s, N-CH$_2$-CH$_2$-C̲H$_2$-CH$_3$). TGA: $T_{5\% \text{ onset}}$ = 274 °C. DSC: No thermal transitions were observed in the targeted range.

N-butyl-N-methyl-pyrrolidinium nitrocyanamide ([Pyrr$_{14}$][NCA]). ^{1}H NMR (500 MHz, *DMSO-d6*) δ ppm: 3.44 (m, 4H, -C̲H$_2$-N-C̲H$_2$-), 3.30 (m, 2H, N-C̲H$_2$-CH$_2$-CH$_2$-CH$_3$), 2.98 (s,

3H, N-CH$_3$), 2.08 (m, 4H, -C$\underline{H}_2$-C$\underline{H}_2$-), 1.68 (quintet, 2H, N-CH$_2$-C$\underline{H}_2$-CH$_2$-CH$_3$), 1.33 (sextet, 2H, N-CH$_2$-CH$_2$-C$\underline{H}_2$-CH$_3$), 0.94 (t, 3H, N-CH$_2$-CH$_2$-CH$_2$-C$\underline{H}_3$); ^{13}C NMR (125 MHz, DMSO-*d6*) δ ppm: 117.3 (s, O$_2$N-N-C≡N), 63.9 (s, $\underline{C}$H$_2$-N-$\underline{C}$H$_2$-), 63.5 (N-$\underline{C}$H$_2$-CH$_2$-CH$_2$-CH$_3$), 47.9 (s, N-CH$_3$), 25.5 (N-CH$_2$-$\underline{C}$H$_2$-CH$_2$-CH$_3$), 21.6 (s, -C$\underline{H}_2$-C$\underline{H}_2$-), 19.8 (s, N-CH$_2$-CH$_2$-$\underline{C}$H$_2$-CH$_3$), 13.9 (s, N-CH$_2$-CH$_2$-$\underline{C}$H$_2$-CH$_3$). TGA: $T_{\text{5% onset}}$ = 270 $^{\text{o}}$C. DSC: No thermal transitions were observed in the targeted range.

N-butyl-N-methyl-pyrrolidinium azide ([Pyrr$_{14}$][N$_3$]). ^{1}H NMR (500 MHz, *DMSO-d6*) δ ppm: 3.45 (m, 4H, -C$\underline{H}_2$-N-C$\underline{H}_2$-), 3.31 (m, 2H, N-C$\underline{H}_2$-CH$_2$-CH$_2$-CH$_3$), 3.00 (s, 3H, N-CH$_3$), 2.08 (m, 4H, -C$\underline{H}_2$-C$\underline{H}_2$-), 1.68 (quintet, 2H, N-CH$_2$-C$\underline{H}_2$-CH$_2$-CH$_3$), 1.32 (sextet, 2H, N-CH$_2$-CH$_2$-C$\underline{H}_2$-CH$_3$), 0.93 (t, 3H, N-CH$_2$-CH$_2$-CH$_2$-C$\underline{H}_3$); ^{13}C NMR (125 MHz, DMSO-*d6*) δ ppm: 63.8 (s, $\underline{C}$H$_2$-N-$\underline{C}$H$_2$-), 63.4 (N-$\underline{C}$H$_2$-CH$_2$-CH$_2$-CH$_3$), 47.9 (s, N-CH$_3$), 25.5 (N-CH$_2$-$\underline{C}$H$_2$-CH$_2$-CH$_3$), 21.6 (s, -C$\underline{H}_2$-C$\underline{H}_2$-), 19.8 (s, N-CH$_2$-CH$_2$-$\underline{C}$H$_2$-CH$_3$), 13.9 (s, N-CH$_2$-CH$_2$-$\underline{C}$H$_2$-CH$_3$). TGA: $T_{\text{5% onset}}$ = 175 $^{\text{o}}$C. DSC: No thermal transitions were observed in the targeted range.

N-allyl-N-methyl-pyrrolidinium dicyanamide ([Pyrr$_{1A}$][DCA]). ^{1}H NMR (500 MHz, *DMSO-d6*) δ ppm: 6.07 (ddt, 1H, CH$_2$-C$\underline{H}$=CH$_2$), 5.63 (dd, 1H, =CH$_2$ *cis* to C-H), 5.61 (dd, 1H, =CH$_2$ *trans* to C-H), 3.97 (d, 2H, N-C$\underline{H}_2$-CH=CH$_2$), 3.43 (m, 4H, -C$\underline{H}_2$-N-C$\underline{H}_2$-), 2.97 (s, 3H, N-CH$_3$), 2.09 (m, 4H, -C$\underline{H}_2$-C$\underline{H}_2$-); ^{13}C NMR (125 MHz, DMSO-*d6*) δ ppm: 127.4 (s, -$\underline{C}$H=CH$_2$), 127.2 (s, -CH=$\underline{C}$H$_2$), 119.3 (s, N-C≡N), 65.2 (s, N-$\underline{C}$H$_2$-CH=CH$_2$), 63.4 (s, -$\underline{C}$H$_2$-N-$\underline{C}$H$_2$-), 48.5 (s, N-CH$_3$), 21.7 (s, -C$\underline{H}_2$-C$\underline{H}_2$-). TGA: $T_{\text{5% onset}}$ = 249 $^{\text{o}}$C. DSC: T_c = -64 $^{\text{o}}$C, T_m = -21 $^{\text{o}}$C.

N-methyl-N-allyl-pyrrolidinium nitrocyanamide ([Pyrr$_{1A}$][NCA]). ^{1}H NMR (500 MHz, *DMSO-d6*) δ ppm: 6.07 (ddt, 1H, CH$_2$-C$\underline{H}$=CH$_2$), 5.63 (dd, 1H, =CH$_2$ *cis* to C-H), 5.61 (dd, 1H, =CH$_2$ *trans* to C-H), 3.97 (d, 2H, N-C$\underline{H}_2$-CH=CH$_2$), 3.44 (m, 4H, -C$\underline{H}_2$-N-C$\underline{H}_2$-), 2.98 (s, 3H, N-CH$_3$), 2.10 (m, 4H, -C$\underline{H}_2$-C$\underline{H}_2$-); ^{13}C NMR (125 MHz, DMSO-*d6*) δ ppm: 127.4 (s, -$\underline{C}$H=CH$_2$), 127.2 (s, -CH=$\underline{C}$H$_2$), 117.2 (s, O$_2$N-N-C≡N), 65.2 (s, N-$\underline{C}$H$_2$-CH=CH$_2$), 63.4 (s, -$\underline{C}$H$_2$-N-$\underline{C}$H$_2$-), 48.5 (s, N-CH$_3$), 21.7 (s, -C$\underline{H}_2$-C$\underline{H}_2$-). TGA: $T_{\text{5% onset}}$ = 258 $^{\text{o}}$C. DSC: No thermal transitions were observed in the targeted range.

N-allyl-N-methyl-pyrrolidinium azide ([Pyrr$_{1A}$][N$_3$]). ^{1}H NMR (500 MHz, *DMSO-d6*) δ ppm: 6.07 (ddt, 1H, CH$_2$-C$\underline{H}$=CH$_2$), 5.64 (dd, 1H, =CH$_2$ *cis* to C-H), 5.59 (dd, 1H, =CH$_2$ *trans* to C-H), 4.02 (d, 2H, N-C$\underline{H}_2$-CH=CH$_2$), 3.49 (m, 4H, -C$\underline{H}_2$-N-C$\underline{H}_2$-), 3.00 (s, 3H, N-CH$_3$), 2.09 (m, 4H, -C$\underline{H}_2$-C$\underline{H}_2$-); ^{13}C NMR (125 MHz, DMSO-*d6*) δ ppm: 127.4 (s, -$\underline{C}$H=CH$_2$), 127.3 (s, -CH=$\underline{C}$H$_2$), 65.1 (s, N-$\underline{C}$H$_2$-CH=CH$_2$), 63.3 (s, -$\underline{C}$H$_2$-N-$\underline{C}$H$_2$-), 48.3 (s, N-CH$_3$), 21.7 (s, -C$\underline{H}_2$-

C$\underline{H}_2$-). TGA: $T_{5\% \text{ onset}}$ = 158 ^{o}C. DSC: No thermal transitions were observed in the targeted range.

N-butyl-3-methyl-pyridinium dicyanamide ([C$_4$C$_1$py][DCA]). ^{1}H NMR (500 MHz, *DMSO-d6*) δ ppm: 9.00 (s, 1H, between N and Me), 8.92 (d, 1H, C-H *ortho* to N), 8.45 (d, 1H, C-H *para* to N), 8.06 (t, 1H, C-H *meta* to N), 4.55 (t, 2H, N-C$\underline{H}_2$-CH$_2$-CH$_2$-CH$_3$), 3.32 (s, 3H, C-CH$_3$), 1.90 (quintet, 2H, N-CH$_2$-C$\underline{H}_2$-CH$_2$-CH$_3$), 1.30 (sextet, 2H, N-CH$_2$-CH$_2$-C$\underline{H}_2$-CH$_3$), 0.92 (t, 3H, N-CH$_2$-CH$_2$-CH$_2$-C$\underline{H}_3$); ^{13}C NMR (125 MHz, DMSO-*d6*) δ ppm: 146.5 (s, C between N and Me), 144.6 (s, C *ortho* to N), 142.3 (s, $\underline{C}$-CH$_3$), 139.0 (s, C *para* to N), 127.8 (s, C *meta* to N), 119.8 (s, N-C≡N), 60.8 (s, N-$\underline{C}$H$_2$-CH$_2$-CH$_2$-CH$_3$), 32.8 (s, C-$\underline{C}$H$_3$), 19.7 (s, N-CH$_2$-$\underline{C}$H$_2$-CH$_2$-CH$_3$), 18.2 (s, N-CH$_2$-CH$_2$-$\underline{C}$H$_2$-CH$_3$), 14.1 (s, N-CH$_2$-CH$_2$-CH$_2$-$\underline{C}$H$_3$). TGA: $T_{5\% \text{ onset}}$ = 249 ^{o}C. DSC: T_m = 20 ^{o}C.

N-butyl-3-methyl-pyridinium nitrocyanamide ([C$_4$C$_1$py][NCA]). ^{1}H NMR (500 MHz, *DMSO-d6*) δ ppm: 9.00 (s, 1H, between N and Me), 8.92 (d, 1H, C-H *ortho* to N), 8.45 (d, 1H, C-H *para* to N), 8.06 (t, 1H, C-H *meta* to N), 4.55 (t, 2H, N-C$\underline{H}_2$-CH$_2$-CH$_2$-CH$_3$), 3.32 (s, 3H, C-CH$_3$), 1.90 (quintet, 2H, N-CH$_2$-C$\underline{H}_2$-CH$_2$-CH$_3$), 1.30 (sextet, 2H, N-CH$_2$-CH$_2$-C$\underline{H}_2$-CH$_3$), 0.92 (t, 3H, N-CH$_2$-CH$_2$-CH$_2$-C$\underline{H}_3$); ^{13}C NMR (125 MHz, DMSO-*d6*) δ ppm: 146.5 (s, C between N and Me), 144.6 (s, C *ortho* to N), 142.3 (s, $\underline{C}$-CH$_3$), 139.0 (s, C *para* to N), 127.8 (s, C *meta* to N), 117.3 (s, O$_2$N-N-C≡N), 60.8 (s, N-$\underline{C}$H$_2$-CH$_2$-CH$_2$-CH$_3$), 32.8 (s, C-$\underline{C}$H$_3$), 19.7 (s, N-CH$_2$-$\underline{C}$H$_2$-CH$_2$-CH$_3$), 18.2 (s, N-CH$_2$-CH$_2$-$\underline{C}$H$_2$-CH$_3$), 14.1 (s, N-CH$_2$-CH$_2$-CH$_2$-$\underline{C}$H$_3$). TGA: $T_{5\% \text{ onset}}$ = 265 ^{o}C. DSC: T_g = -79 ^{o}C.

N-butyl-3-methyl-pyridinium azide ([C$_4$C$_1$py][N$_3$]). ^{1}H NMR (500 MHz, *DMSO-d6*) δ ppm: 9.06 (s, 1H, between N and Me), 8.97 (d, 1H, C-H *ortho* to N), 8.46 (d, 1H, C-H *para* to N), 8.05 (t, 1H, C-H *meta* to N), 4.58 (t, 2H, N-C$\underline{H}_2$-CH$_2$-CH$_2$-CH$_3$), 3.44 (s, 3H, C-CH$_3$), 1.90 (quintet, 2H, N-CH$_2$-C$\underline{H}_2$-CH$_2$-CH$_3$), 1.29 (sextet, 2H, N-CH$_2$-CH$_2$-C$\underline{H}_2$-CH$_3$), 0.90 (t, 3H, N-CH$_2$-CH$_2$-CH$_2$-C$\underline{H}_3$); ^{13}C NMR (125 MHz, DMSO-*d6*) δ ppm: 146.2 (s, C between N and Me), 144.8 (s, C *ortho* to N), 142.4 (s, $\underline{C}$-CH$_3$), 139.3 (s, C *para* to N), 127.8 (s, C *meta* to N), 60.9 (s, N-$\underline{C}$H$_2$-CH$_2$-CH$_2$-CH$_3$), 33.0 (s, C-$\underline{C}$H$_3$), 19.2 (s, N-CH$_2$-$\underline{C}$H$_2$-CH$_2$-CH$_3$), 18.3 (s, N-CH$_2$-CH$_2$-$\underline{C}$H$_2$-CH$_3$), 13.8 (s, N-CH$_2$-CH$_2$-CH$_2$-$\underline{C}$H$_3$). TGA: $T_{5\% \text{ onset}}$ = 166 ^{o}C. DSC: T_g = -79 ^{o}C.

N-allyl-pyridinium dicyanamide [Apy][DCA]. ^{1}H NMR (500 MHz, *DMSO-d6*) δ ppm: 9.04 (d, 2H, C-H *ortho* to N), 8.64 (t, 1H, C-H *para* to N), 8.19 (t, 2H, C-H *meta* to N), 6.18 (ddt, 1H, CH$_2$-C$\underline{H}$=CH$_2$), 5.47 (dd, 1H, =CH$_2$ *cis* to C-H), 5.41 (dd, 1H, =CH$_2$ *trans* to C-H), 5.28 (d,

2H, N-C$\underline{H}_2$-CH=CH$_2$); ^{13}C NMR (125 MHz, DMSO-*d6*) δ ppm: 146.4 (s, C *ortho* to N), 145.3 (s, C-*para* to N), 132.1 (C *meta* to N), 128.7 (s, -$\underline{C}$H=CH$_2$), 122.4 (s, -CH=$\underline{C}$H$_2$), 119.6 (s, N-C≡N), 62.9 (s, N-$\underline{C}$H$_2$-CH=CH$_2$). TGA: $T_{5\% \text{ onset}}$ = 170 ^{o}C. DSC: No thermal transitions were observed in the targeted range.

_N_-allyl-pyridinium nitrocyanamide [Apy][NCA]. ^{1}H NMR (500 MHz, *DMSO-d6*) δ ppm: 9.06 (d, 2H, C-H *ortho* to N), 8.65 (t, 1H, C-H *para* to N), 8.20 (t, 2H, C-H *meta* to N), 6.18 (ddt, 1H, CH$_2$-C$\underline{H}$=CH$_2$), 5.47 (dd, 1H, =CH$_2$ *cis* to C-H), 5.42 (dd, 1H, =CH$_2$ *trans* to C-H), 5.29 (d, 2H, N-C$\underline{H}_2$-CH=CH$_2$); ^{13}C NMR (125 MHz, DMSO-*d6*) δ ppm: 146.4 (s, C *ortho* to N), 145.3 (s, C-*para* to N), 132.1 (C *meta* to N), 128.7 (s, -$\underline{C}$H=CH$_2$), 122.4 (s, -CH=$\underline{C}$H$_2$), 117.3 (s, O$_2$N-N-C≡N), 62.9 (s, N-$\underline{C}$H$_2$-CH=CH$_2$). TGA: $T_{5\% \text{ onset}}$ = 210 ^{o}C. DSC: T_g = -80 ^{o}C.

_N_-allyl-pyridinium azide ([Apy][N$_3$]). ^{1}H NMR (500 MHz, *DMSO-d6*) δ ppm: 9.08 (d, 2H, C-H *ortho* to N), 8.65 (t, 1H, C-H *para* to N), 8.20 (t, 2H, C-H *meta* to N), 6.18 (ddt, 1H, CH$_2$-C$\underline{H}$=CH$_2$), 5.45 (dd, 1H, =CH$_2$ *cis* to C-H), 5.42 (dd, 1H, =CH$_2$ *trans* to C-H), 5.31 (d, 2H, N-C$\underline{H}_2$-CH=CH$_2$); ^{13}C NMR (125 MHz, DMSO-*d6*) δ ppm: 146.3 (s, C *ortho* to N), 145.3 (s, C-*para* to N), 132.1 (C *meta* to N), 128.7 (s, -$\underline{C}$H=CH$_2$), 122.4 (s, -CH=$\underline{C}$H$_2$), 62.9 (s, N-$\underline{C}$H$_2$-CH=CH$_2$). TGA: $T_{5\% \text{ onset}}$ = 110 ^{o}C. DSC: No thermal transitions were observed in the targeted range.

Acknowledgements

References

1   Smiglak, M.; Metlen, A.; Rogers, R. D. *Acc. Chem. Res.* **2007**, *40*, 1182-1192.
2   Zhang. Y.; Gao, H.; Joo, Y-H.; Shreeve, J. M. *Angew. Chem. Int. Ed.* **2011**, *50*, 9554-9562.
3   Schneider, S.; Hawkins, T.; Rosander, M.; Vaghjiani, G.; Chambreau, S.; Drake, G. *Energy & Fuels* **2008**, *22*, 2871-2872.
4   He, Tao, G-H.; Parrish, D. A.; Shreeve, J. M. *Chem. Eur. J.* **2010**, *16*, 5736-5743.
5   Zhang, Y.; Shreeve, J. M. *Angew. Chem. Int. Ed.* **2011**, *50*, 935-937.
6   Clark, J. D. *Ignition: An Informal History of Liquid Rocket Propellants*, Rutgers University Press: New Brunswick, NJ, 1972.

7   Schneider, S.; Hawkins, T.; Ahmed, Y.; Rosander, M.; Hudgens, L.; Mills, J. *Angew.Chem. Int. Ed.* **2011**, *50*, 5886-5888.

8   Wang, K.; Zhang, Y.; Chand, D.; Parrish, D. A.; Shreeve, J. M. *Chem. Eur. J.* **2012**, *18*, 16931-16937.

9   McCrary, P. D.; Beasley, P. A.; Alaniz, S. A.; Griggs, C. S.; Frazier, R. M. Rogers, R. D. *Angew. Chem. Int. Ed.* **2012**, *51*, 9784-9787.

10   Schneider, S.; Hawkins, T.; Ahmed, Y.; Deplazes, S.; Mills, J. Ionic Liquids for Chemical Propulsion. In *Ionic Liquids: Science and Applications*; Visser, A. E.; Bridges, N. J.; Rogers, R. D., Eds.; American Chemical Society: Washington, DC, 2012.

11   Chambreau, S. D.; Schneider, S.; Rosander, M.; Hawkins, T.; Gallegos, C. J.; Pastewalt, M. F.; Vaghjiani, G. L. *J. Phys. Chem. A.* **2008**, *112*, 7816-7824.

12   Koh, C. J.; Liu, C-L.; Harmon, C. W.; Strasser, D.; Golan, A.; Kostko, O.; Chambreau, S. D.; Vaghjiani, G. L.; Leone, S. R. *J. Phys. Chem. A* **2011**, *115*, 4630-4635.

13   Litzinger, T.; Iyer, S. *Energy Fuels* **2011**, *25*, 72-76.

14   Chingin, K.; Perry, R. H.; Chambreau, S. D.; Vaghjiani, G. L.; Zare, R. N. *Angew. Chem. Int. Ed.* **2011**, *50*, 8634-8637.

15   Catorie, L.; Chambreau, S. D.; Vaghjiani, G. L. *Combust. Flame* **2012**, *159*, 1759-1768.

16   Schneider, S.; Hawkins, T.; Rosander, M.; Mills, J.; Brand, A.; Hudgens, L.; Warmoth, G.; Vij, A. *Inorg. Chem.* **2008**. *47*, 3617-3624.

17   Schneider, S.; Hawkins, T.; Rosander, M.; Mills, J.; Vaghjiani, G.; Chambreau, S. *Inorg. Chem.* **2008**, *47*, 6082-6089.

18   Schneider, S.; Drake, G.; Hall, L.; Hawkins, T.; Rosander, M. *Z. Anorg. Allg. Chem.* **2007**, *633*, 1701-1707.

19   Zare, P.; Stojanovic, A.; Herbst, F.; Akbarzadeh, J.; Peterlik, H.; Binder, W. H. *Macromolecules* **2012**, *45*, 2074-2084.

20   Zhang, H.; Wu, J.; Zhang, J.; He, J. *Macromolecules* **2005**, *38*, 8772-8277.

21   Avent, A. G.; Chaloner, P. A.; Day, M. P.; Seddon, K. R. Welton, T. *J. Chem. Soc. Dalton Trans.* **1994**, 3405-3413.

22   McCrary, P. D.; Beasley, P. A.; Cojocaru, O. A.; Schneider, S.; Hawkins, T. W.; Perez, J. P. L.; McMahon, B. W.; Pfiel, M.; Boatz, J. A.; Anderson, S. L.; Son, S. F.; Rogers, R. D. *Chem. Commun.* **2012**, *48*, 4311-4313.

23   Bonhôte, P.; Dias, A-P.; Papageorgiou, N.; Kalyanasundaram, K.; Grätzel, M. *Inorg. Chem.* **1996**, *35*, 1168-1178.

24   Liu, Q.; Janssen, M. H. A.; van Rantwijk, F.; Sheldon, R. A. *Green Chem.* **2005**, *39-42*.

25   Laus, G.; Bentivoglio, G.; Kahlenberg, V.; Griesser, U. J.; Schottenberger, H.; Nauer, G. *CrystEngComm* **2008**, *10*, 748-752.

26   Yim, T.; Lee, H. Y.; Kim, H-J.; Mun, J.; Kim, S.; Oh, S. M.; Kim, Y. G. *Bull. Korean Chem. Soc.* **2007**, *28*, 1567-1572.

27   Jiang, N.; Pu, Y.; Samuel, R.; Ragauskas, A. J. *Green Chem.* **2009**, *11*, 1762-1766.

28   Huddleston, J. G.; Visser, A. E.; Reichert, W. M.; Willauer, H. D.; Broker, G. A.; Rogers, R. D. *Green Chem.* **2001**, *3*, 156-164.

29   MacFarlane, D. R.; Golding, J.; Forsyth, S.; Forsyth, M.; Deacon, G. B. *Chem. Commun.* **2001**, 1430-1431.

30   MacFarlane, D. R.; Forsyth, S. A.; Golding, J.; Deacon, G. B. *Green Chem.* **2002**, *4*, 444-448.

31   Zhao, D.; Fei, Z.; Geldbach, T. J.; Scopellitii, R.; Dyson, P. J. *J. Am. Chem. Soc.* **2004**, *126*, 15876-15882.

32   Zhao, D.; Fei, Z.; Scopelliti, R.; Dyson, P. J. *Inorg. Chem.* **2004**, *43*, 2197-2205.

33   Fredlake, C. P.; Crosthwaite, J. M.; Hert, D. G.; Aki, S. N. V. K.; Brennecke, J. F. *J. Chem. Eng. Data* **2004**, *49*, 954-964.

34   Wooster, T. J.; Johanson, K. M.; Fraser, K. J.; MacFarlane, D. R.; Scott, J. L. *Green. Chem.* **2006**, *6*, 691-696.

35   Yoshida, Y.; Baba, O.; Saito, G. *J. Phys. Chem. B* **2007**, *111*, 4742-4749.

36   Sanchez, L. G.; Espel, J. R.; Onink, F.; Meindersma, G. W.; de Haan, A. B. *J. Chem. Eng. Data* **2009**, *54*, 2803-2812.

37   Meine, N.; Benedito, F.; Rinalidi, R. *Green Chem.* **2010**, *12*, 1711-1714.

38   Ngo, H. L.; LeCompte, K.; Hargens, L.; McEwen, A. B. *Thermochim. Acta* **2000**, *357-358*, 97-102.

39   Tang, S.; Baker, G. A.; Zhao, H. *Chem. Soc. Rev.* **2012**, *41*, 4030-4066.

40   Monteiro, M. J.; Camilo, F. F.; Ribiero, M. C. C.; Torresi, R. M. *J. Phys. Chem. B.* **2010**, *113*, 12488-12494.

41   Kim, J.; Singh, R. P.; Shreeve, J. M. *Inorg. Chem.* **2004**, *43*, 2960-2966.

42   Joo, Y-H.; Gao, H.; Zhang, Y.; Shreeve, J. M. *Inorg. Chem.* **2010**, *49*, 3282-3288.

43   Fei, Z.; Kuang, D.; Zhao, D.; Klein, C.; Ang, W. H.; Zakeeruddin, S. M.; Grätzel, M.; Dyson, P. J. *Inorg. Chem.* **2006**, *45*, 10407-10409.

44   Zhao, D.; Fei, Z.; Ang, W. H.; Dyson, P. J. *Int. J. Mol. Sci.* **2007**, *8*, 304-315.

45   Singh, R. P.; Verma, R. D.; Meshri, D. T.; Shreeve, J. M. *Angew. Chem. Int. Ed.* **2006**, *45*, 3584-3601.

46   Spengler, V. G.; Bauer, J. *Brennstoff-Chemie* **1965**, *4*, 43-50.

47   Sheldrick, G. M. *SHELXTL, structure determination software suite,* **2003**, v.6.14, Bruker AXS Inc: Madison, WI.

48   Sheldrick, G. M. *SHELXL, structure determination software suite,* **2013**, v. 2013/4, Bruker AXS Inc: Madison, WI.

49   Sheldrick, G. M. *Acta Cryst.* **2008**, *A64*, 112-122.

50   Macrae, F.; Bruno, I. J.; Shisholm, J. A.; Edgington, P. R.; McCabe, P.; Picock, E.; Rodriguez-Monge, L.; Taylor, R.; van de Streek, J.; Wood, P. A. *J. Appl. Cryst.* **2008**, *41*, 4660-4670.

51   Macrae, C. F.; Edgington, P. R.; McCabe, P.; Pidcock, E.; Shields, G. P.; Taylor, R.; Towler, M.; van de Streek, J. *J. Appl. Cryst.* **2006**, *39*, 453-457.

52   Harris, S. R. *J. Am. Chem. Soc.* **1958**, *80*, 2302-2305.

Evaluating Ionic Liquids as Hypergolic Fuels: Predicting Reactivity from Molecular Structure

Parker D. McCrary, Gregory Chatel,[‡] Spencer A. Alaniz, O. Andreea Cojocaru, Preston A. Beasley,[§] Luis A. Flores, Steven P. Kelley, Patrick S. Barber, and Robin D. Rogers*

Center for Green Manufacturing and Department of Chemistry, The University of Alabama, Tuscaloosa, AL 35487, USA.

[‡]Current Address: Institut de Chimie des Milieux et Matériaux de Poitiers (IC2MP), CNRS/Université de Poitiers, ENSIP, Bat. B1, 1 rue Marcel Doré, 86073 Poitiers Cedex 9, France.

[§]Current Address: Power Systems and Environmental Research, Southern Research Institute, 2000 Ninth Ave. S., Birmingham, AL 35205, USA.
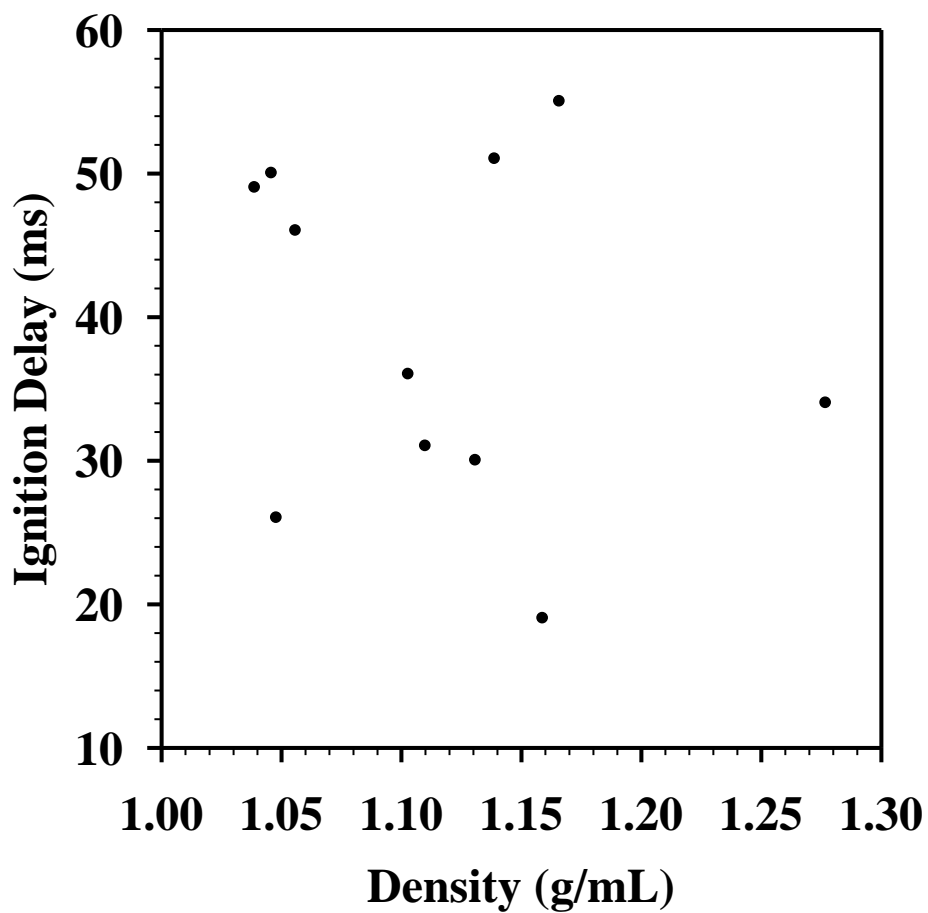
Table of Contents

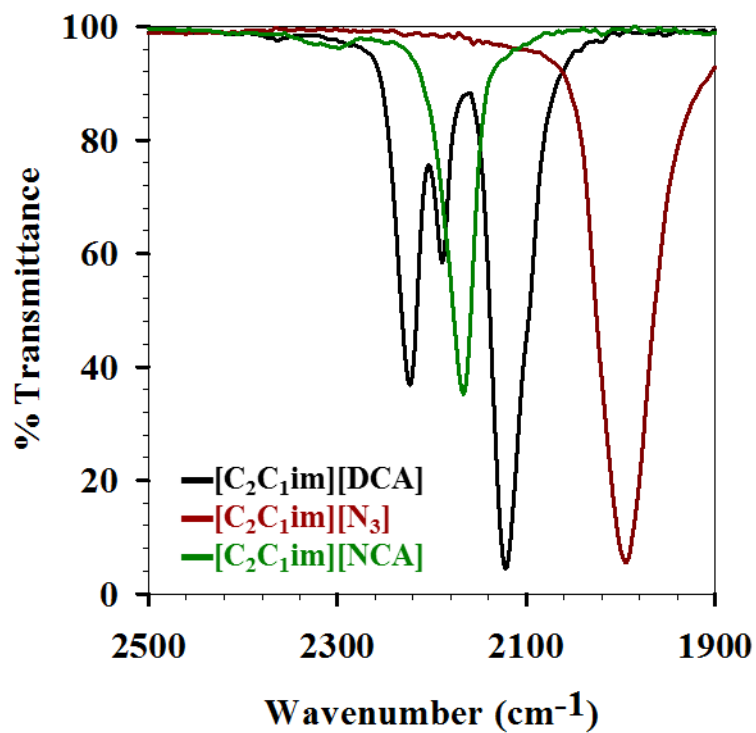**I.   Density and Viscosity *vs*. Ignition Delay**
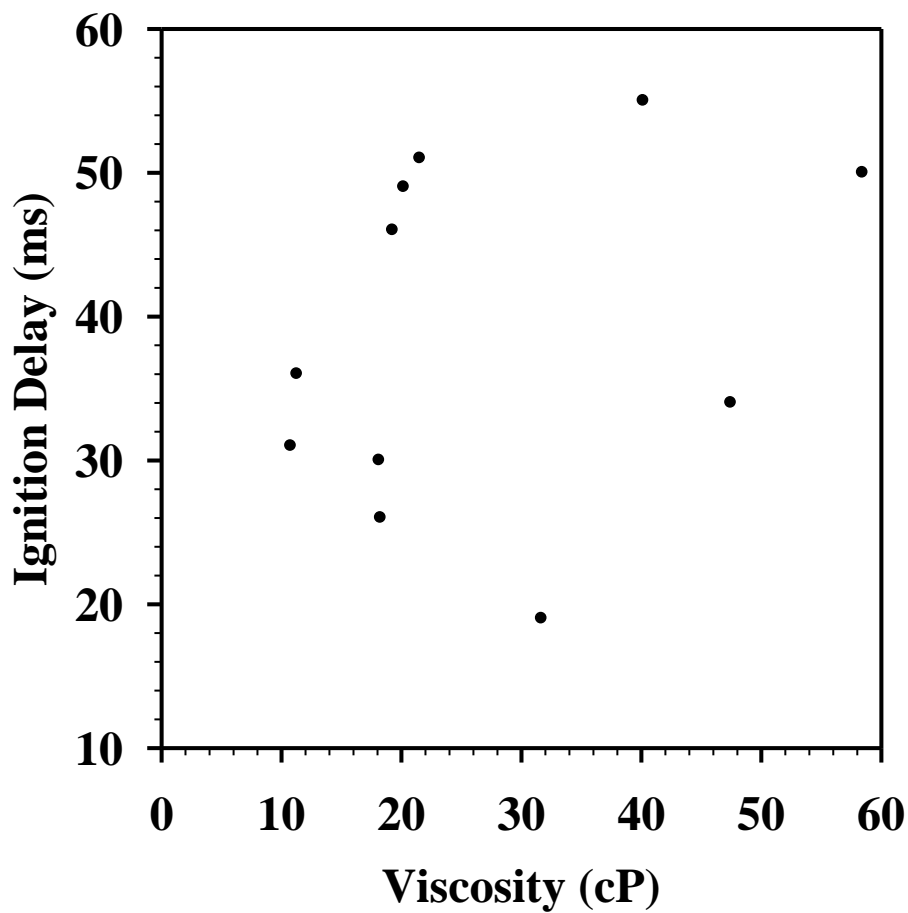
Figure S1. Viscosity of hypergolic [DCA]⁻-based ILs *vs*. ignition delay
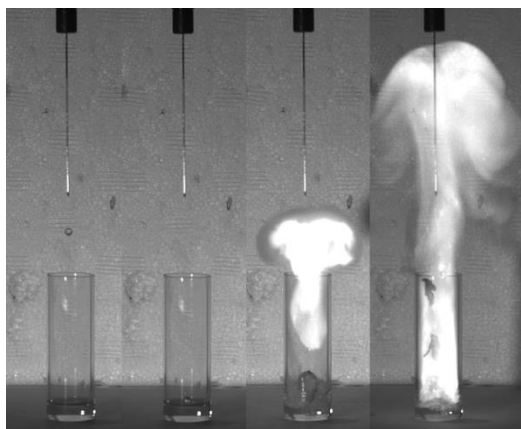
Figure S2. Density of hypergolic [DCA]⁻-based ILs *vs.* ignition delay

II.   IR Spectra of Anionic Species

Figure S3. IR spectra of key functional groups in the [DCA]⁻ (all C≡N stretches), [N₃]⁻ (all N=N stretches), and [NCA]⁻ (C≡N stretch) anions

Evaluating Ionic Liquids as Hypergolic Fuels: Exploring Reactivity from Molecular Structure†

Parker D. McCrary, Gregory Chatel, Spencer A. Alaniz, O. Andreea Cojocaru, Preston A. Beasley, Luis A. Flores, Steven P. Kelley, Patrick S. Barber, and Robin D. Rogers*

A study of hypergolicity in 38 ionic liquids suggested that reactivity is strongly correlated to increased electron density in the cation, with small changes in physical properties having little effect beyond a certain threshold.